# Chapter 4. Application of SEAM3D to a Field Site

## 4.1 Introduction

SEAM3D was applied to a subsurface spill of gasoline from underground storage tanks at the Laurel Bay Exchange, Marine Corps Air Station, Beaufort, S.C. Site records indicate that the spill probably began in late 1990. Site measurements indicated that gasoline had spread along the water table as a nonaqueous phase liquid (NAPL) and created a continuing source of groundwater contamination. Electron acceptors (EAs) available at the site included oxygen ($O_2$), ferric iron (Fe(III)), sulfate ($SO_4^{2-}$), and carbon dioxide ($CO_2$). Nitrate ($NO_3^-$) concentrations were measured at the site and found to be too low to degrade significant amounts of hydrocarbon. Groundwater samples taken in 1994 indicated that biodegradation of BTEX was occurring with $O_2$ and Fe(III) acting as EAs (Landmeyer et al., 1996). Fe(II) production was observed only in locations where $O_2$ was depleted, suggesting $O_2$ inhibition of Fe(III)-based biodegradation. No sulfide ($H_2S$) or methane ($CH_4$) production was measured in 1994, but additional data collected in 1996 and 1997 showed significant concentrations of $H_2S$ and $CH_4$ and elevated levels of molecular hydrogen ($H_2$). This indicated that sulfate reduction and methanogenesis had begun at least four years after the contamination occurred.

Gasoline is a complex mixture of dozens of organic compounds, and the composition of gasoline varies with time of year, manufacturer, and octane level (Sigsby et al., 1987). Therefore, gasoline contains numerous substrates that can utilize EAs. In order to accurately model EA depletion, it is important to account for all biodegradable substrates. Otherwise, the model will overpredict the amount of EA available to react with the compounds of interest such as BTEX. For example, if a gasoline spill occurs and benzene only is simulated, then the model allows all available EA mass to react with the benzene. In reality, other hydrocarbons from the gasoline are utilized and prevent a certain percentage of the EAs from biodegrading with benzene. For modeling purposes, it is impractical to simulate all components of gasoline individually. Therefore, it is common practice (Baehr and Corapcioglu, 1987; Rixey et al., 1991; Rixey and Dortch, 1992) to lump certain compounds together and create a simplified NAPL representative of gasoline (Table 4.1). For example, it may be reasonable to lump all aliphatics together since they generally have low solubility and are utilized only under aerobic conditions. For these

simulations, the BTEX compounds were treated individually because toluene tends to biodegrade preferentially relative to the others; not all BTEX biodegrade using all of the EAs simulated; and the predicted benzene concentration is typically the basis for regulatory decisions on intrinsic bioremediation.

Table 4.1. Mass fraction of various components of gasoline, as measured or used in simulations by the researchers listed.

| Component | Sigsby et al. (1987) No-lead Regular | Sigsby et al. (1987) No-lead Premium | Baehr and Corapcioglu (1987) | Rixey et al. (1991) | Parr et al. (1991) | Rixey and Dorch (1992) |
|---|---|---|---|---|---|---|
| | (%) | (%) | (%) | (%) | (%) | (%) |
| benzene | 1.76 | 1.96 | 1.14 | 1.0 | 1.94 | 1.0 |
| toluene | 5.54 | 20.25 | 6.07 | 7.0 | 4.73 | 5.0 |
| ethylbenzene | 1.17 | 0.94 | -- | 9.0* | 2.00 | 10.0 |
| xylene | 7.04 | 4.21 | -- | -- | 9.65 | -- |
| total aromatics | 31.23 | 44.2 | 27.52 | 39.0 | -- | 36.0 |
| total aliphatics | 68.77 | 55.8 | 52.26 | 61.0 | -- | 64.0 |
| heavy ends | -- | -- | 20.21 | -- | -- | -- |

* total of ethylbenzene and xylene

## 4.2 Site Description

The contaminated site is located at the Laurel Bay Exchange, Marine Corps Air Station, Beaufort, S.C. A continuing source of groundwater contamination resulted when gasoline leaked from storage tanks at the Marine Corps Exchange (MCEX) Service Station. Details of the site history and hydrogeology have been published previously (ABB Environmental Services, 1993; Landmeyer et al., 1996), so this section will serve to summarize information relevant to the modeling effort.

### *4.2.1 NAPL source history*

Three underground gasoline storage tanks (Figure 4.1) were installed at the MCEX site in 1973. The tanks were first tested for tightness by the overfill method in December, 1989, but the results were inconclusive for all three tanks. Tanks 1537 and 1538 failed a test for tightness by the underfill method in December, 1990, and in September, 1991, two inches of NAPL was observed in monitoring well LB-EX-1. In November, 1991, tanks 1536 and 1537 were determined to be tight, but tank 1538 was still leaking, so it was emptied and taken out of service. A total of approximately 0.095 $m^3$ (25 gallons) of NAPL was bailed out of LB-EX-1 from October, 1991 until March, 1993, with NAPL thickness in the well ranging from 10 to 90 cm. In April, 1993, ABB Environmental Services (ABB-ES) investigated the area to determine the horizontal and vertical extent of contamination. Based on observation of visible NAPL sheen and analysis of soil cores, ABB-ES estimated that NAPL occupied a circular area approximately 22 m in diameter (Figure 4.1). Thus, NAPL had migrated in the direction of the water table gradient from the immediate vicinity of the tanks. In late 1993, the tanks and surrounding sediments were removed (Landmeyer et al., 1996).

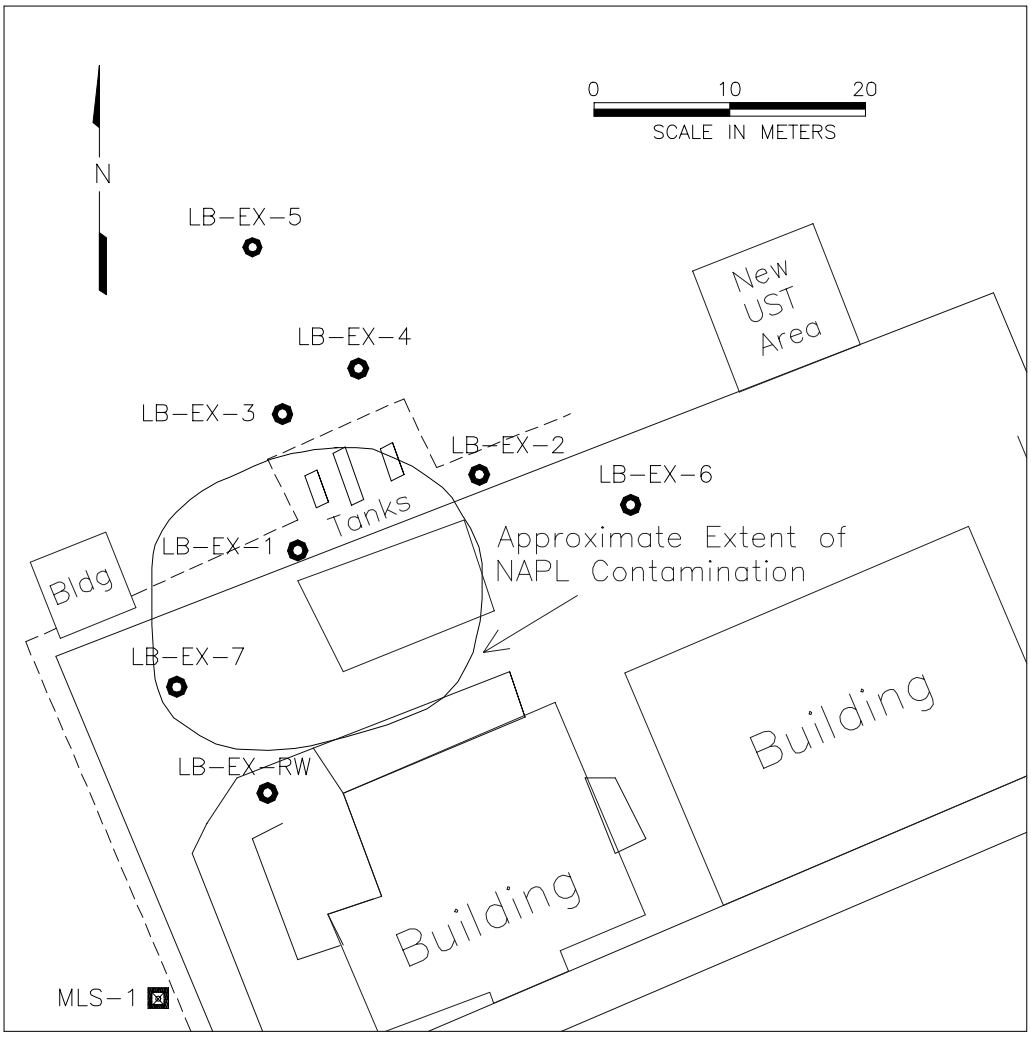


Figure 4–1. Site map of the Laurel Bay Exchange, Marine Corps Air Station, Beaufort, S.C., showing location of the leaking gasoline storage tanks and the estimated extent of non–aqueous phase contamination in 1993.

### *4.2.2 Field monitoring*

During their site investigation, ABB-ES drilled 27 soil borings to the water table and installed 12 shallow groundwater monitoring wells (LB-EX-5 through 16) screened over the water table. The screened interval below the water table varied from 2.52 to 3.79 m, depending on the water table elevation and the well location. In addition to the shallow wells, a deep well (LB-EX-17) was installed in the base of the aquifer next to LB-EX-8 (Figure 4.2) to provide an estimate of the vertical gradient in piezometric head and the vertical extent of contaminant migration. ABB-ES measured concentrations of benzene, toluene, ethylbenzene, total xylenes (BTEX), and methyl-tert-butyl-ether (MTBE) in the soil vapor, water, and solids. In March, 1994, the United States Geological Survey (USGS) continued the site investigation and installed monitoring wells LB-EX-18 to LB-EX-22 (Figure 4.2). The USGS tested the groundwater for BTEX and MTBE, and also measured concentrations of potential EAs ($O_2$, $NO_3^-$, $SO_4^{2-}$) and products of biodegradation (ferrous iron (Fe(II)), sulfide ($H_2S$), methane ($CH_4$), $H_2$, and dissolved inorganic carbon (DIC)). In order to obtain addition data on the vertical distribution of contamination, two multilevel sampling (MLS) wells were installed at the site in October, 1995, and four additional multilevel samplers (Figures 4.2 and 4.3) were installed in June, 1996. The USGS measured concentrations of BTEX, EAs, and products again in June, 1996 and January, 1997. Due to the relatively low elevation of the water table in June, 1996, only the lower ports of the multilevel samplers (Table 4.2) could be sampled. In January, 1997, MLS-1 was the only multilivel sampler from which measurements were obtained.

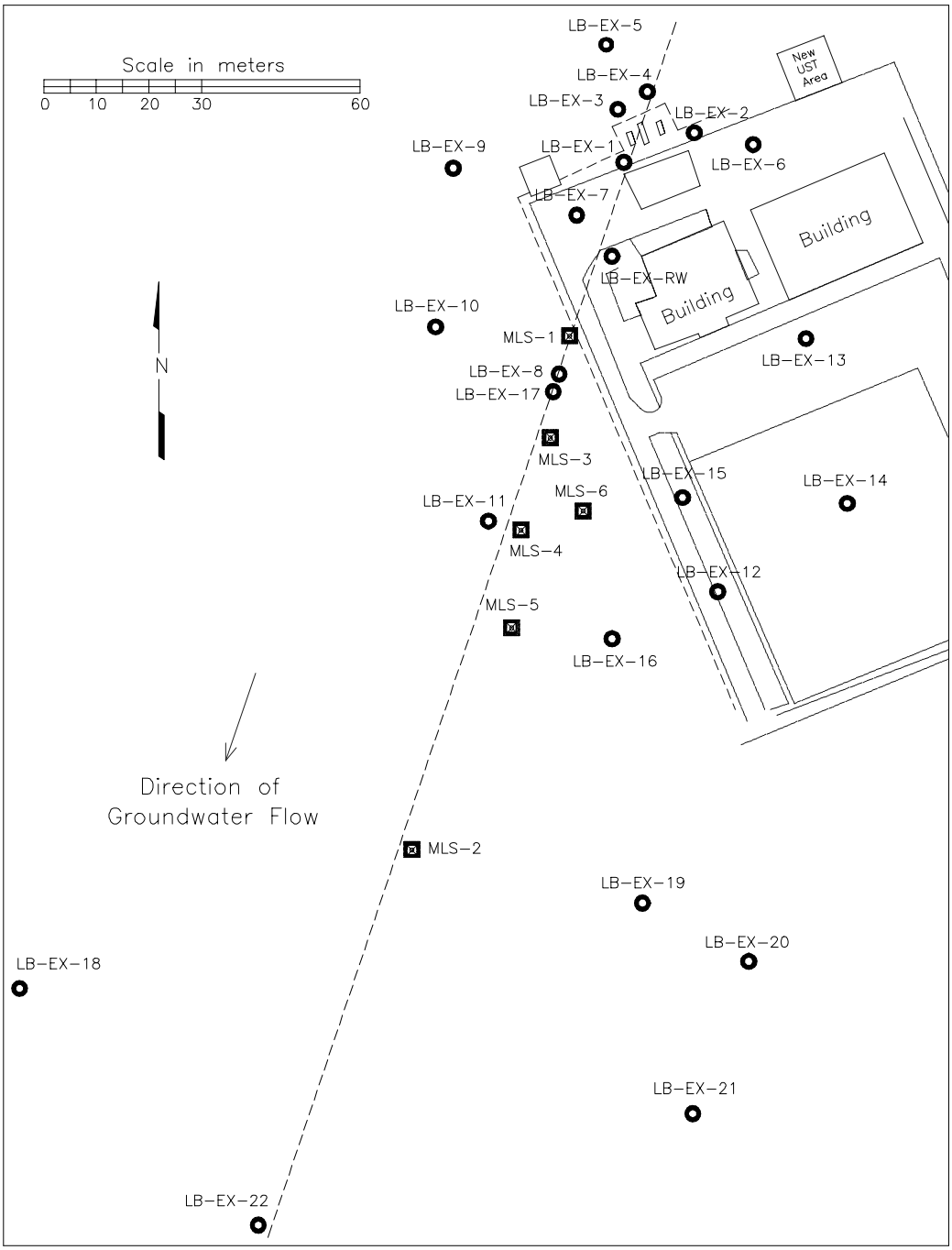


Figure 4–2. Location of monitoring wells and multilevel samplers at the Laurel Bay gasoline spill site. The dashed line marks the transect through the center of the plume.

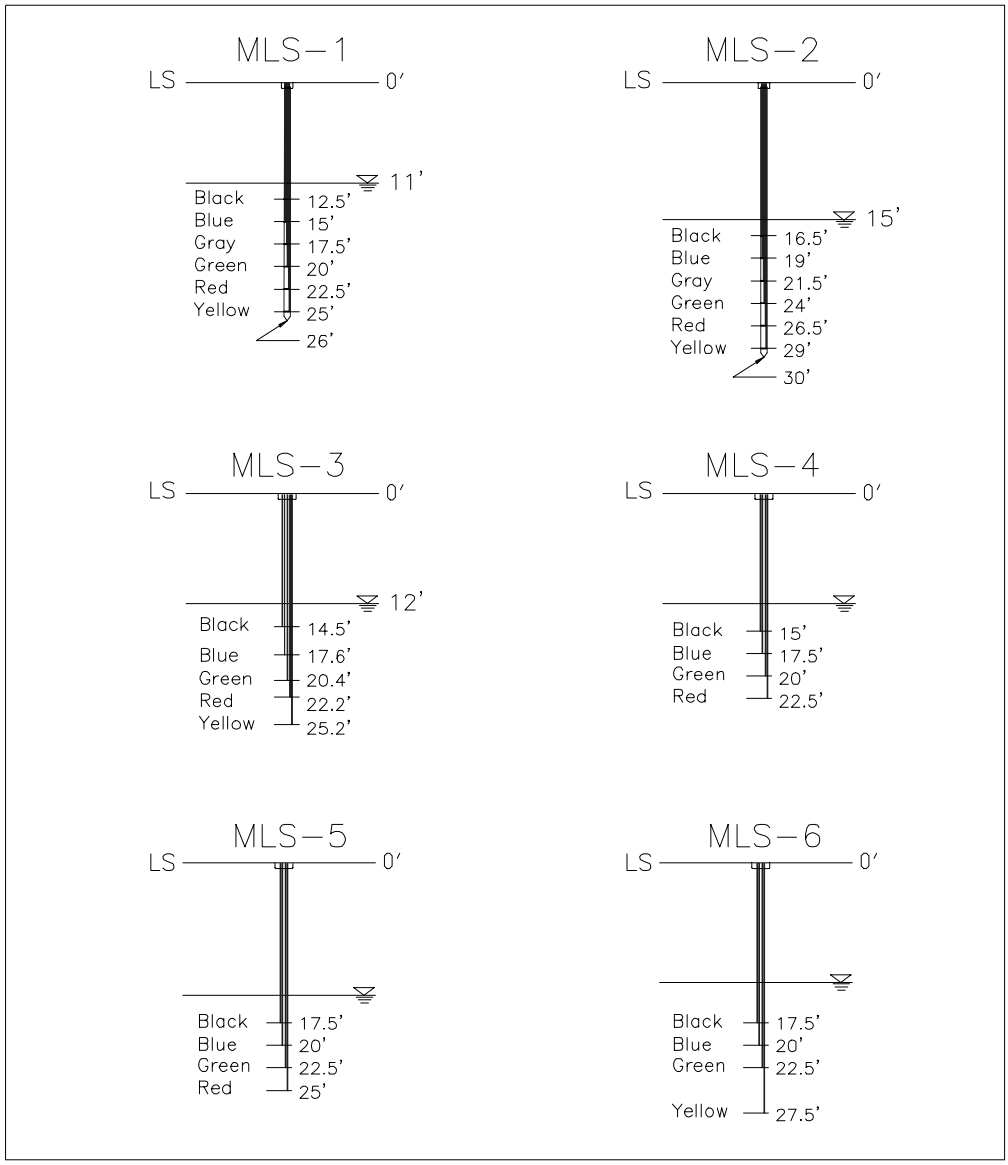


Figure 4–3. Installation details of the multilevel samplers (MLS–1 to MLS–6) used to monitor the vertical distribution of contamination. The color code for the sampling tubes is indicated, and the depth below land surface (LS) is given.

Table 4.2. Concentrations of BTEX, MTBE, electron acceptors and products of biodegradation measured in the multilevel sampling wells on June 25, 1996. Port depth refers to depth below the 1996 water table.

| Well # | Port depth | Benzene | Toluene | Ethyl benzene | Total Xylene | MTBE | $O_2$ | $SO_4^{2-}$ | Fe(II) | $H_2S$ | $CH_4$ |
|---|---|---|---|---|---|---|---|---|---|---|---|
| | (m) | ($g\,m^{-3}$) | ($g\,m^{-3}$) | ($g\,m^{-3}$) | ($g\,m^{-3}$) | ($g\,m^{-3}$) | ($g\,m^{-3}$) | ($g\,m^{-3}$) | ($g\,m^{-3}$) | ($g\,m^{-3}$) | ($g\,m^{-3}$) |
| MLS1 | 2.0 | -- | -- | -- | -- | -- | -- | 1.58 | 4.94 | 13.6 | -- |
| | 2.7 | 5.80 | 22.7 | 3.06 | 9.45 | 0.69 | 0.00 | 0.07 | 4.67 | 1.10 | 0.20 |
| | 3.5 | 7.09 | 21.4 | 3.33 | 9.69 | 22.9 | 0.00 | 0.13 | 4.90 | 4.30 | 0.40 |
| MLS3 | 2.5 | -- | -- | -- | -- | -- | -- | 18.6 | 10.3 | 0.20 | 0.60 |
| | 3.4 | 0.73 | 0.30 | 0.41 | 0.57 | 2.20 | 0.00 | 3.49 | 2.31 | 30.0 | -- |
| MLS4 | 0.6 | -- | -- | -- | -- | -- | -- | 39.8 | 4.86 | 0.40 | 0.20 |
| | 1.3 | -- | -- | -- | -- | -- | 0.00 | 2.5 | 4.65 | 0.10 | 0.20 |
| | 2.1 | 9.40 | 0.02 | 1.13 | 2.43 | 102.0 | 0.00 | 4.09 | 4.26 | 10.8 | 0.20 |
| MLS5 | 1.1 | -- | -- | -- | -- | -- | 0.91 | 9.45 | 0.29 | 0.00 | -- |
| | 1.9 | 0.06 | 0.28 | 0.01 | 0.04 | 2.18 | 1.04 | 10.9 | 2.06 | 0.00 | -- |
| | 2.6 | 0.10 | 0.13 | 0.02 | 0.06 | 2.34 | 1.25 | 10.4 | 1.68 | 0.00 | -- |
| MLS6 | 2.7 | -- | -- | -- | -- | -- | 0.00 | 25.5 | 4.64 | 0.0 | 0.20 |
| | 4.2 | 1.34 | 2.00 | 0.22 | 0.59 | 19.2 | 0.00 | 7.52 | 4.15 | 0.0 | 0.10 |

### *4.2.3 Hydrogeology*

The unconfined Atlantic Coastal Plain aquifer at the MCEX site is comprised mostly of fine-grained silty sand (ABB Environmental Services, 1993). The depth from the ground surface to the regional confining unit is approximately 12 m, while the depth to the water table averages 3 m. Thus the saturated thickness of the aquifer is approximately 9 m. Measurements of the water table elevations at the site have revealed water table fluctuations of less than 1 m, although fluctuations of 2 m have been reported in the general area (ABB Environmental Services, 1993). ABB-ES performed slug tests on LB-EX-6, 13, 14, and 16 and calculated a geometric mean hydraulic conductivity of 3.383 m $day^{-1}$ for the aquifer. The horizontal water table gradient was estimated as 0.0059 in 1993, 0.0046 in 1994, and 0.0059 in 1996. The vertical gradient in piezometric head was estimated as 0.023 in 1993 and 0.017 in 1996, based on measured water levels in shallow well LB-EX-08 and deep well LB-EX-17.

### *4.2.4 Laboratory investigations*

Landmeyer et al. (1996) measured adsorption of benzene and toluene onto aquifer solids, and used a linear model to estimate the distribution coefficient ($K_D$). Values of $K_D$ ranged from 0.057 to 0.14 $cm^3$ $g^{-1}$ for toluene and 0.057 to 0.28 $cm^3$ $g^{-1}$ for benzene. Laboratory measurements of toluene biodegradation were obtained from microcosms containing sediments and groundwater collected near LB-EX-RW and LB-EX-8. Microbial degradation rates under aerobic and anaerobic conditions were estimated from the measured rate of $^{14}CO_2$ production from radiolabeled toluene. The aerobic biodecay rate was estimated as 0.64 $day^{-1}$, while the anaerobic rate was 0.003 $day^{-1}$. The anaerobic biodegradation rate for benzene was estimated as 0.00025 $day^{-1}$ (Landmeyer et al., 1996) using trial and error matching of measured benzene concentrations versus concentrations predicted by the solute transport model SUTRA (Voss, 1984), using first order decay to simulate benzene biodegradation.

## 4.3 SEAM3D Parameter Estimation

All parameters for SEAM3D were initially chosen based on site data or literature values. Subsequently, the model was calibrated to the 1993, 1994, and 1996 data by adjusting a limited

number of parameters to create a match between predicted and observed concentrations of hydrocarbons, EAs, and products. In general, parameters were not adjusted if an accurate measurement was available. Parameters that were allowed to be adjusted included dispersivities, maximum specific rates of substrate utilization ($\nu^{max}_{x,ls,le}$), inhibition coefficients ($\kappa_{le,li}$), and mass fractions of BTEX and other constituents in the NAPL. Only the inhibition coefficients were adjusted using the 1996 data.

### *4.3.1 Model domain and control parameters*

The three-dimensional model domain for flow and transport (Figure 4.4 and 4.5), was 400 m in the longitudinal x-direction, 98 m in the transverse y-direction, and 9 m in the vertical z-direction. The domain was divided into 49 rows, 200 columns, and 9 layers using 2 x 2 x 1 m blocks. The uppermost aquifer layer was specified as unconfined, and the bottom elevation of this layer was given the same slope as the water table. Thus the vertical thickness of the aquifer was uniform. The flow solution was steady state, while the transport simulations were transient, with both the transport time step and the biodegradation time step set to 1.5 days. Time zero for the simulations was chosen as December 15, 1990, when the tanks first failed a test for tightness. For model calibration, simulations ran for 2025 days, to encompass the 1993, 1994, and 1996 data. Predictive simulations ran for 6000 days, although data for comparison were available only for the 1997 data at 2230 days.

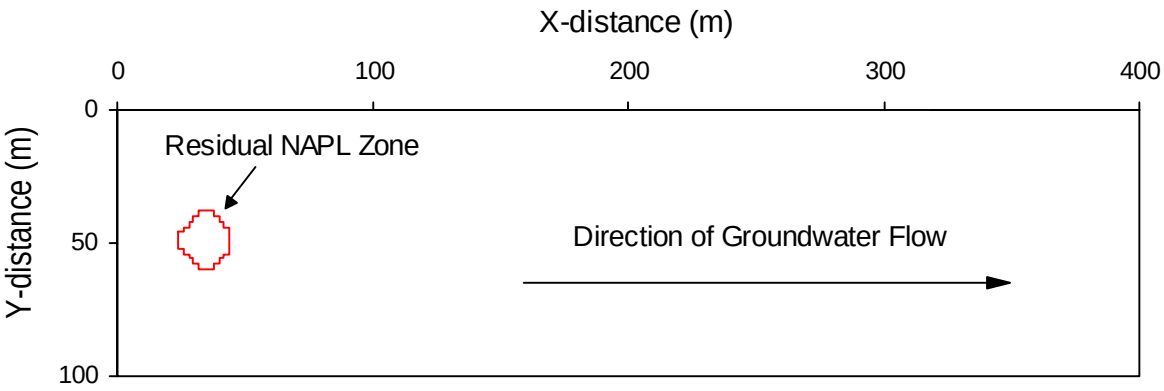


Figure 4.4. Areal view of the SEAM3D model domain used to simulate the Laurel Bay site.

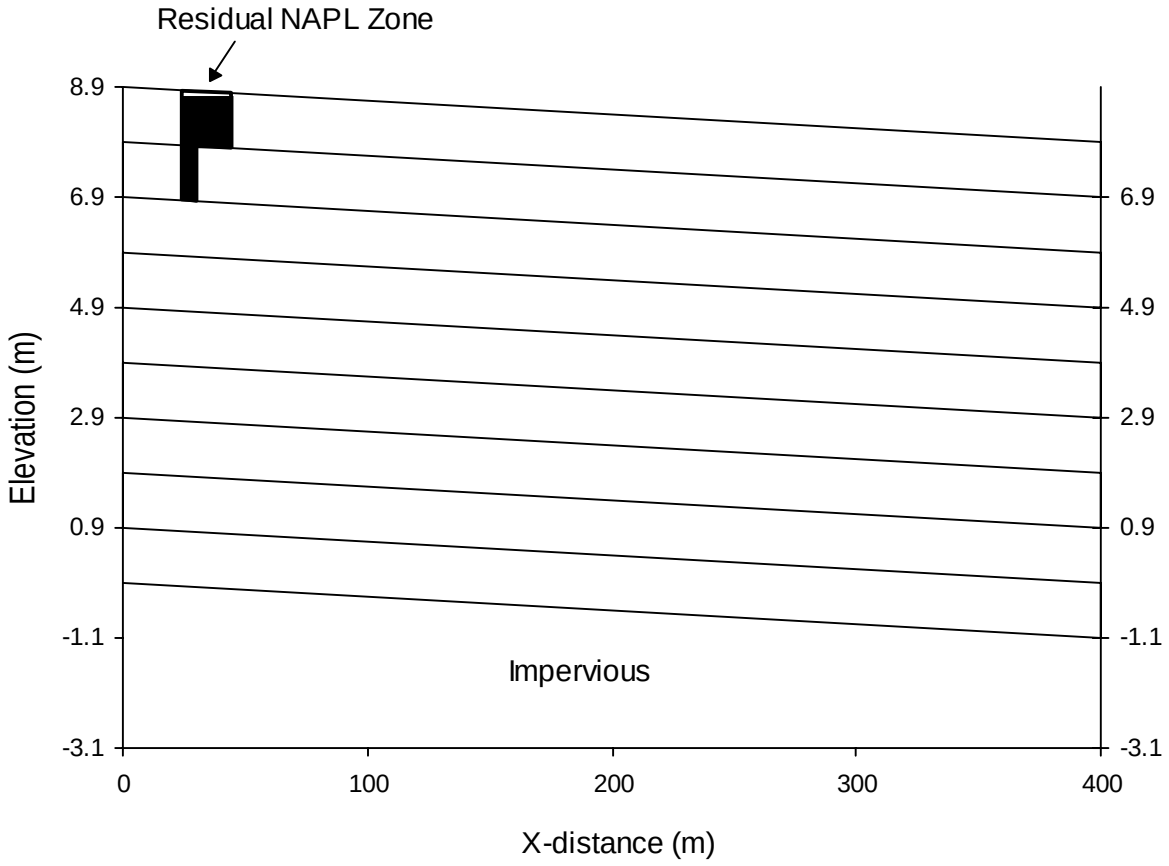


Figure 4.5. Vertical cross section through the SEAM3D model domain used to simulate the Laurel Bay site.

### *4.3.2 Flow parameters and boundary conditions*

The groundwater flow model MODFLOW (McDonald and Harbaugh, 1988) was used to generate the steady state flow field for contaminant transport. The uppermost aquifer layer was given a hydraulic conductivity of 3.383 m $day^{-1}$. Since the vertical thickness of each layer was 1.0 m, the transmissivity for the lower layers was also 3.383 $m^2$ $day^{-1}$. Based on the average gradient (0.005) in the measured water table, the average groundwater velocity was approximately 18 m $yr^{-1}$. The vertical leakance between layers was 0.338 m $day^{-1}$, based on the assumption that the horizontal conductivity was ten times greater than the vertical conductivity. This degree of anisotropy in hydraulic conductivity is not uncommon (Bouwer, 1978). Boundary conditions were no flow along y = 0 and y = 98, and constant head in layer 1 equal to 8.90 m at x = 0 and 7.91 m at x = 200. Assuming a linear head drop with depth over the entire domain, the constant head values at x = 0 and x = 200 were decreased by 0.02 m for each subsequent layer in order to simulate the average vertical gradient measured between LB-EX-08 and LB-EX-17. Recharge at the site was not measured, so a value of 0.00042 m $day^{-1}$ was chosen as a conservative estimate, assuming limitations due to evapotranspiration and runoff. A constant value of recharge was specified for all blocks in layer 1. The combination of the recharge flow and the vertical gradient in the constant head boundaries produced a relatively uniform horizontal gradient of 0.005 in the water table.

### *4.3.3 NAPL contamination*

The gasoline leak was simulated as occurring in the 2 x 2 m block between tanks 1537 and 1538 (Figure 4.1). The beginning date for the simulated leak was designated as December 15, 1990, when the tanks first failed a test for tightness, and the ending date for the leak was November 15, 1991, when tank 1538 was emptied and taken out of service. Thus the duration of the leak was 330 days. NAPL was assumed to have migrated from the immediate vicinity of the tanks to produce the NAPL distribution observed by ABB-ES in 1993. The model does not simulate NAPL flow explicitly, but the effect of NAPL migration was approximated by using schedules to add NAPL to successive blocks as time progressed (Figure 4.6 and Table 4.3). Once the model added NAPL to a block, NAPL mass was diminished only by dissolution into the aqueous phase.

Time values for the NAPL schedules were determined by estimating the average velocity ($v_{NAPL}$) of the NAPL plume as (Parker et al., 1994)

$$v_{NAPL} = M_o \frac{dZ_{ao}}{dx} \tag{4.1}$$

where $M_o$ is the oil mobility factor, and $dZ_{ao}/dx$ is the gradient in the air-oil table, which can be estimated as corresponding to the water table gradient. At high volumes of hydraulically mobile or "free" NAPL per unit volume of soil, $M_o$ reaches a constant maximum value ($M_o^{max}$), computed as

$$M_o^{max} = \frac{\rho_{ro} K_s}{\eta_{ro} \theta} \tag{4.2}$$

where $K_s$ is the saturated hydraulic conductivity of water, $\rho_{ro}$ is the oil specific gravity, $\eta_{ro}$ is the ratio of oil to water viscosity, and $\theta$ is the effective porosity. Research has shown that for gasoline, $\rho_{ro} \cong 0.8$ and $\eta_{ro} \cong 0.6$ (Parker et al., 1994), and the value $\theta = 0.35$ (Table 4.4) was estimated during the initial site investigation (ABB Environmental Services, 1993). Therefore, $M_o^{max}$ was 12.9 m day$^{-1}$. When the free NAPL volume is large, $M_o^{max}$ has been shown to give a reasonable estimate of $v_{NAPL}$ (Parker et al., 1994), while for small free NAPL volumes, the value $M_o^{max}/2$ may provide a better approximation (Parker et al., 1994). Since the observed free NAPL thickness in LB-EX-1 was generally small (ABB Environmental Services, 1993), $M_o^{max}/2$ was used in equation 4.1 to obtain $v_{NAPL} = 0.032$ m day$^{-1}$.

Each model block was 2 x 2 m, and free NAPL migrating at 0.032 m day$^{-1}$ would take 62 days to travel 2 m to the next block. Thus, for blocks adjacent to the leak, NAPL mass loading began on day 62, following schedule 2 (Table 4.3). For blocks furthest from the leak, NAPL had to travel 20 m, so mass loading began on day 620 and continued until day 950, following schedule 11. NAPL mass loading into all blocks lasted for 330 days, under the assumption that free NAPL would continue to migrate as long as the leak persisted.

The mass loading rate for a specific block was based on an estimate of the total NAPL mass assumed to have entered that block. This total mass was derived from field measurements and theoretical worst case NAPL saturations. Field measurements of NAPL concentrations

ranged from 2.3 x $10^{-6}$ to 0.00051 g $g^{-1}$ (ABB Environmental Services, 1993), but none of the samples were taken within 10 m of the leak, where the highest NAPL concentrations were likely to have occurred. To estimate the worst case NAPL concentrations, it was assumed that the NAPL plume in 1993 was essentially immobile, and thus composed entirely of residual NAPL. This assumption was based on the small observed NAPL thickness (about 5 cm) in LB-EX-1 and lack of NAPL in any other monitoring wells. For sandy soils, residual NAPL saturations generally range from 0.05 to 0.20 (Wilson et al., 1990). Thus, the worst case NAPL saturation was taken to be 0.20. Using a soil bulk density of 1.6 x $10^{6}$ g $m^{-3}$ (Table 4.4) and NAPL density of 0.8 x $10^{6}$ g $m^{-3}$, a saturation of 0.20 corresponds to a soil concentration of 0.04 $g_{NAPL}\ g_{solids}^{-1}$. Thus the total NAPL mass in the worst case model blocks was 256 kg. In addition, it was assumed that NAPL concentrations decreased in a linear manner with distance from the leak. For the worst case, the minimum NAPL mass per block was set to 32 kg, which corresponded to a NAPL saturation of 0.025 and a soil NAPL concentration of 0.005 $g_{NAPL}\ g_{solids}^{-1}$. Since the measured soil concentrations were an order of magnitude lower than the worst case estimates, the "best estimate" concentrations were judged to be half of the worst case.

The vertical distribution of the simulated source was based on the observed water table fluctuations of approximately 1 m. Near the leak, observed NAPL thickness ranged up to 0.9 m in LB-EX-1, so it was assumed that water table fluctuations in this area spread NAPL over the upper 2 m of the aquifer. Farther from the leak, NAPL was not observed in any of the monitoring wells, so the free NAPL thickness was assumed to be small. As a result, free NAPL would form a thin layer floating on the water table, and NAPL would not spread beyond the 1 m water table fluctuation. Thus, NAPL mass was loaded to the upper two layers of model blocks near the leak, while the other blocks received NAPL only in the top layer (Figure 4.6). The shaded blocks in Figure 4.6 show those zones (between the source and LB-EX-01) in which the model set NAPL concentration to zero after 1000 days in order to simulate the excavation of the tanks and surrounding sediments.

In gasoline, the BTEX compounds are of primary regulatory interest due to their relatively high solubility and potential toxicity. Therefore, each BTEX compound was simulated individually, while all other aromatics were treated as a single pseudo-compound. Likewise, all

aliphatics were simulated as a single pseudo-compound because they are less soluble in water than BTEX, and they were assumed to degrade aerobically only. MTBE was simulated as an individual component since it was assumed to be nonbiodegradable and unretarded. Hereafter, we will use the term "substrates" to refer to the BTEX, the other biodegradable aromatics, and the aliphatics; and the term "tracer" to refer to MTBE. The mass fractions of the model constituents in the NAPL (Table 4.5) were based on mass fractions of BTEX, other aromatics, aliphatics, and MTBE that are within the range observed in gasoline (see Table 4.1). Mole fractions and solubilities of the aromatic and aliphatic pseudo-compounds were based on estimates made by Baehr and Corapcioglu (1987). No measurements were available to estimate the mass transfer coefficient ($k^{NAPL}$) describing NAPL dissolution to the aqueous phase. Therefore, $k^{NAPL}$ was set to a high value, which allowed the aqueous phase concentration of each NAPL constituent to be equal to its equlibrium value.

Table 4.3. Timing and mass loading information associated with the schedule numbers in Figure 4.6 for NAPL mass loading to the model domain.

| Schedule Number | Mass Loading Letter | NAPL mass loading starting time | NAPL mass loading ending time | NAPL mass loading rate | Total NAPL mass added to block |
|---|---|---|---|---|---|
| | | (day ) | (day ) | ( g / day ) | ( kg ) |
| 1 | A | 0 | 330 | 338 | 128 |
| 2 | A | 62 | 392 | 338 | 128 |
| | B | | | 291 | 96 |
| 3 | B | 124 | 454 | 291 | 96 |
| 4 | C | 186 | 516 | 194 | 64 |
| 5 | C | 248 | 578 | 194 | 64 |
| | D | | | 97 | 32 |
| 6 | D | 310 | 640 | 97 | 32 |
| | E | | | 48 | 16 |
| 7 | D | 372 | 702 | 97 | 32 |
| | E | | | 48 | 16 |
| 8 | D | 434 | 764 | 97 | 32 |
| | E | | | 48 | 16 |
| 9 | D | 496 | 826 | 97 | 32 |
| | E | | | 48 | 16 |
| 10 | E | 558 | 888 | 48 | 16 |
| 11 | E | 620 | 950 | 48 | 16 |

Table 4.4. Transport parameters representing longitudinal dispersivity ($\alpha_x$), transverse dispersivity ($\alpha_y$), vertical dispersivity ($\alpha_z$), effective porosity ($\theta$), and soil bulk density ($\rho_b$).

| $\alpha_x$ | $\alpha_y$ | $\alpha_z$ | $\theta$ | $\rho_b$ |
|---|---|---|---|---|
| ( m ) | ( m ) | ( m ) | ( - ) | ( $g\ m^{-3}$ ) |
| 8.0 | 1.2 | 0.04 | 0.35 | $1.6 \times 10^6$ |

Table 4.5. Properties and composition of the NAPL phase used in the simulations.

| Component | Initial Mass Fraction in NAPL | Aqueous Phase Solubility | Molecular Weight |
|---|---|---|---|
| | ($g\ g^{-1}$) | ($g\ m^{-3}$) | ($g\ mole^{-1}$) |
| benzene | 0.01 | 1780 | 78.1 |
| toluene | 0.08 | 515 | 92.1 |
| ethylbenzene | 0.05 | 140 | 106.2 |
| xylene | 0.12 | 180 | 106.2 |
| other aromatics | 0.10 | 166 | 120.0 |
| aliphatics | 0.55 | 12 | 97.0 |
| inert | 0.06 | 0 | 150.0 |
| MTBE | 0.03 | 20,000 | 80.0 |

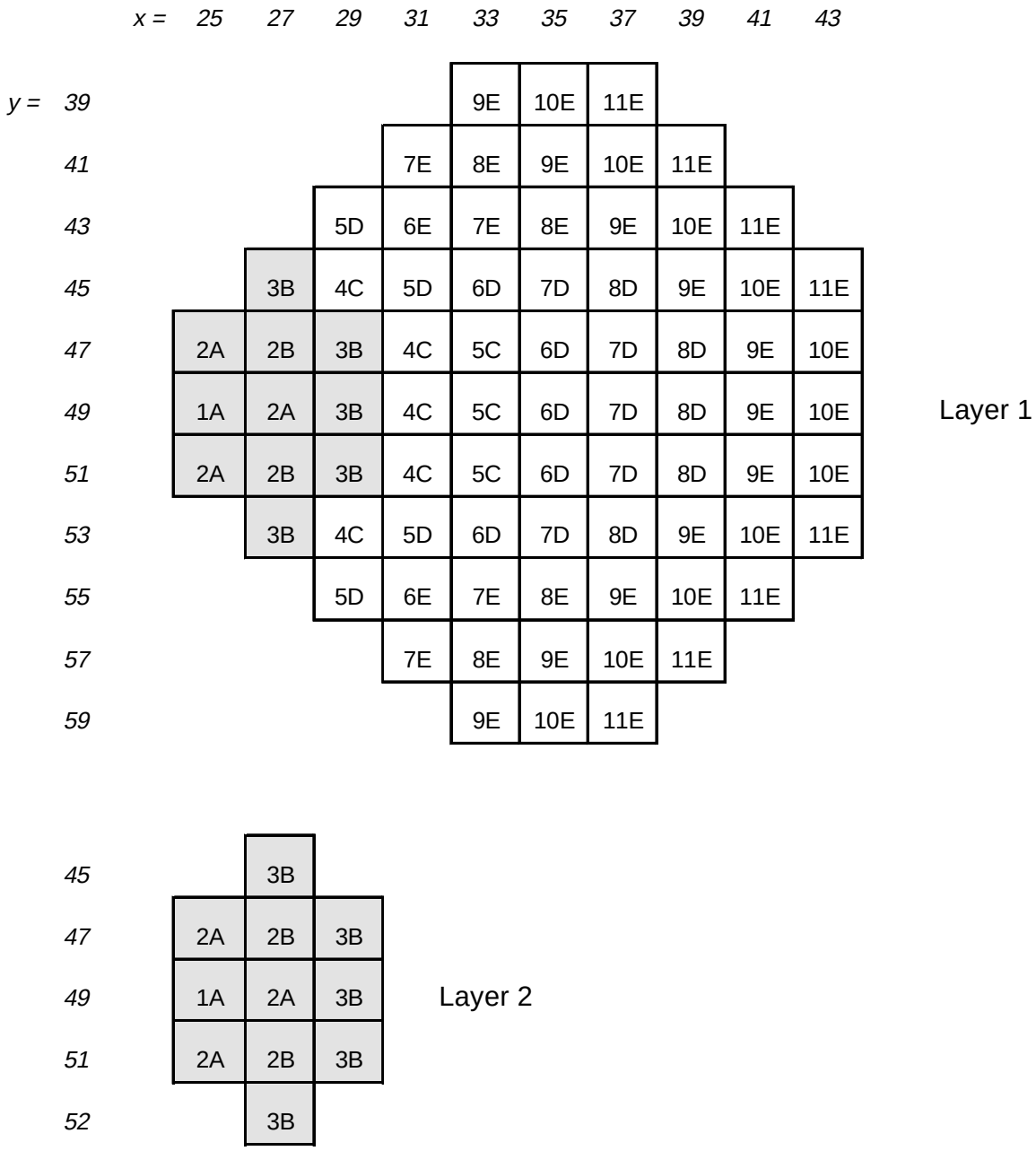


Figure 4.6. Location of the NAPL source within the model domain. The values of *x* and *y* indicate the distance to the center of the model blocks. Within each block, the number refers to the schedule (see Table 4.3) for adding NAPL to the domain, while the letter refers to the mass loading rate (Table 4.3). Shading indicates those blocks in which the NAPL mass was set to zero at 1000 days to correspond to excavation of the tanks and contaminated soil.

### *4.3.4 Transport parameters and boundary conditions*

Input values for initial concentrations were based on measurements taken from uncontaminated wells at the site (ABB Environmental Services, 1993; Landmeyer et al., 1996). At all nodes, initial concentrations were 5.0 g $m^{-3}$ for oxygen ($O_2$) and 100 μg $g^{-1}$ for solid phase Fe(III), the latter representing only the bioavailable or microbially reducible iron. For sulfate ($SO_4^{2-}$), initial concentrations were 5.0 g $m^{-3}$ at x = 0 and 10.0 g $m^{-3}$ at x = 400. Initial concentrations were zero for all substrates, products, and MTBE. Threshold concentrations (below which biodegradation will not occur) were set to 10 μg $g^{-1}$ for Fe(III) and zero for all other components. Specified concentrations in recharge water were 5.0 g $m^{-3}$ for $O_2$, 15.0 g $m^{-3}$ for $SO_4^{2-}$, and zero for all substrates, products, and MTBE. Boundary conditions were specified as constant concentration equal to the initial condition at x = 0 for all aqueous phase constituents. All other blocks were allowed to be active with variable concentrations. If a solute reached the outflow boundary of the domain, solute mass was allowed to exit under a zero dispersion boundary condition.

The longitudinal dispersitivity ($\alpha_x$) was initially chosen to be 10 m, which was 10% of the overall transport distance during the calibration time period. During calibration, the values for the dispersivities were refined by assuming that MTBE was recalcitrant and adjusting the dispersivities to match the measured data. Thus, $\alpha_x$ (Table 4.4) was reduced by 20%, and it was always assumed that the transverse dispersivity was $0.15\alpha_x$ and the vertical dispersivity was $0.005\alpha_x$. The effect of lowering the dispersivities was to produce a more conservative prediction of biodegradation, as less dispersion allowed less access to the electron acceptors (EAs). The soil bulk density (Table 4.4) was chosen as typical of a sandy soil (see Carsel and Parrish, 1988). The model option for the linear adsorption isotherm was used in calculating retardation factors for each substrate and Fe(II). The electron acceptors, MTBE, $H_2S$, and $CH_4$ were not retarded. To allow for maximum mobility, the distribution coefficient ($k_D$) for all substrates was chosen to be 0.057 cm $g^{-1}$, which was the smallest of the values measured by Landmeyer et al. (1996) for benzene and toluene. For Fe(II), $k_D$ was set to 0.328 $cm^3$ $g^{-1}$ using trial and error adjustments to fit the measured data. Thus the retardation factor was 1.26 for all substrates and 2.5 for Fe(II).

### *4.3.5 Biodegradation parameters*

Model parameters for biodegradation (Tables 4.6 and 4.7) were based on laboratory measurements, published values, and theoretical estimates. For simplicity, parameters values were not allowed to vary among the aquifer layers under the assumption that the entire 9 m of the aquifer could be considered relatively near the surface. In order to reflect the high rate and energy yield of aerobic metabolism, parameters controlling aerobic utilization, growth, and death were higher than those of the anaerobic processes (Tables 4.6 and 4.7). In general, parameters were identical for each substrate and for each anaerobic process unless information existed to assign distinct values.

For aerobic biodecay, the maximum specific rate of substrate utilization ($\nu^{max}_{x,ls,le}$) was set to 0.64 $day^{-1}$ (Table 4.7), based on the laboratory estimate by Landmeyer et al. (1996). Likewise, for anaerobic biodecay, $\nu^{max}_{x,ls,le}$ was initially set to 0.0003 $day^{-1}$ for benzene and 0.003 $day^{-1}$ for all other aromatics, under the assumption that the other aromatics would degrade at a rate similar to toluene. During calibration, $\nu^{max}_{x,ls,le}$ was increased by a factor of four for methanogens and three for the sulfate and iron reducers (Table 4.6) in order to match measured concentrations. This anaerobic rate is still quite low compared to the aerobic decay rate. Alkanes were assumed to be resistant to anaerobic biodecay, so $\nu^{max}_{x,ls,le}$ of the alkanes was set to zero in each anaerobic process (Table 4.7). Values for half saturation coefficients (Table 4.6) were based on literature values since no measurements were available.

The initial microbial biomass ($M_x$) was higher for the aerobes than the iron or sulfate reducers (Table 4.6). This difference was based on the assumption that aerobic biomass would predominate when the groundwater contained significant $O_2$ under pristine conditions. The aerobic biomass of 0.3 g $m^{-3}$ roughly corresponded to 1 x $10^6$ cells $cm^{-3}$, assuming a cell volume of 1 $\mu m^3$ and cell density of 1.0 g $cm^{-3}$. This number of cells and the high $\nu^{max}_{x,ls,le}$ for $O_2$ allowed significant aerobic utilization of substrates to occur immediately. In contrast, anaerobic microbes under high $O_2$ pristine conditions were assumed to exist only in anaerobic microenvironments that develop within soil aggregates (Brock et al., 1994). Thus, the concentrations of iron and sulfate reducers were over an order of magnitude lower than the aerobic biomass (Table 4.6). As a

result, the iron and sulfate reducers had to experience growth before the population exerted a significant impact on biodegradation. For the methanogens, biomass growth was not simulated. Since the model does not explicitly consider an electron acceptor for methanogens, their biomass concentration is limited only by the concentration of available substrate. When substrate is readily available, the methanogenic biomass and the rate of methanogenesis can become unrealistically high if growth is simulated. Therefore, in this case, the yield coefficient and the death rate for methanogens were set to zero, and the initial biomass concentration was set equal to the effective porosity (Table 4.6). Thus the rate of methanogenesis depended only on the maximum specific rate of substrate utilization ( $\nu^{max}_{x,ls,le}$ ) and the concentration of available substrate.

The yield coefficient ($Y_{x,ls,le}$) for aerobes was set to 0.5 g $g^{-1}$ (Table 4.6) based on measurements and past work by Arcangeli and Arvin (1992), Chen et al. (1992), and Wodzinski and Johnson (1968). For all anaerobes, $Y_{x,ls,le}$ was 0.2 g $g^{-1}$, corresponding to the theoretical maximum yield under sulfate reducing conditions (Edwards et al., 1992). Values for the effective death term ( $k^{bk}_{d_x}$ ) were higher for the aerobes than the anaerobes (Table 4.6), reflecting the dependence of $k^{bk}_{d_x}$ on $\nu^{max}_{x,ls,le}$ and $Y_{x,ls,le}$. Inhibition coefficients were relatively small, such that each EA was essentially depleted before utilization of the next EA began. Values for the inhibition coefficients were adjusted during calibration to match measured $H_2S$ and $CH_4$ concentrations. EA use coefficients ($\gamma_{x,ls,le}$) were estimated from the stoichiometric relationship between each EA and toluene (e.g. Borden et al., 1995) and the generation term for methane ($\zeta_{x,ls}$) was based on the stoichiometric relationship between toluene and methane (Borden et al., 1995). The EA generation terms ($\zeta_{x,ls}$) were also based on stoichiometric relationships (Borden et al., 1995; Edwards et al., 1992). During calibration, the generation term for Fe(II) was reduced from its theoretical value to match the measured concentrations of Fe(II). This reduction may be justified since Fe(II) can react chemically with compounds such as $SO_4^{2-}$, so only a fraction of the Fe(II) produced by the microbes will be measured in the groundwater (Lovley et al., 1994).

Table 4.6. Biodegradation parameters representing substrate half saturation constant ($K^{s}_{x,ls,le}$), electron acceptor (EA) half saturation constant ($K^{e}_{x,le}$), yield coefficient ($Y_{x,ls,le}$), EA use coefficient ($\gamma_{x,ls,le}$), inhibition coefficient ($\kappa_{le,li}$), generation coefficient ($\zeta_{x,li}$), initial biomass concentration ($M_x$), and background death rate ($k^{bk}_{d_x}$) for each microbial population. Parameters apply to all substrates.

| Microcolony | EA | $K^{s}_{x,ls,le}$ | $K^{e}_{x,le}$ | $Y_{x,ls,le}$ | $\gamma_{x,ls,le}$ | $\kappa_{le,li}$ | $\zeta_{x,li}$ | $M_x$ | $k^{bk}_{d_x}$ |
|---|---|---|---|---|---|---|---|---|---|
| | | ( $g\ m^{-3}$ ) | ( $g\ m^{-3}$ ) | ( $g\ g^{-1}$ ) | ( $g\ g^{-1}$ ) | ( $g\ m^{-3}$ ) | ( $g\ g^{-1}$ ) | ( $g\ m^{-3}$ ) | ( $day^{-1}$ ) |
| Aerobes | $O_2$ | 5.0 | 0.5 | 0.5 | 3.2 | 0.1 | -- | 0.30 | 0.29 |
| Iron reducers | Fe(III) | 5.0 | -- | 0.2 | 42.0 | 10* | 0.2 | 0.01 | 0.0012 |
| Sulfate reducers | $SO_4$ | 5.0 | 0.5 | 0.2 | 4.5 | 0.5 | 0.8 | 0.01 | 0.0012 |
| Methanogens | $CO_2$ | 5.0 | -- | 0.0 | -- | -- | 0.8 | 0.35 | 0.0 |

* Units are $\mu g$ Fe(III) $g^{-1}$ solids

Table 4.7. Maximum specific rate of substrate utilization ($\nu^{max}_{x,ls,le}$) within each microbial population.

| Microcolony | EA | Benzene | Toluene | Ethyl Benzene | Total Xylene | Other Aromatics | Aliphatics |
|---|---|---|---|---|---|---|---|
| | | ( $day^{-1}$ ) | ( $day^{-1}$ ) | ( $day^{-1}$ ) | ( $day^{-1}$ ) | ( $day^{-1}$ ) | ( $day^{-1}$ ) |
| Aerobes | $O_2$ | 0.640 | 0.640 | 0.640 | 0.640 | 0.640 | 0.640 |
| Iron reducers | Fe(III) | 0.0009 | 0.009 | 0.009 | 0.009 | 0.009 | 0.0 |
| Sulfate reducers | $SO_4$ | 0.0009 | 0.009 | 0.009 | 0.009 | 0.009 | 0.0 |
| Methanogens | $CO_2$ | 0.0003 | 0.003 | 0.003 | 0.003 | 0.003 | 0.0 |

### *4.3.6 SEAM3D calibration*

SEAM3D predictions were compared to measured data from wells (LB-EX-1, 3, 4, 5, 7, 8, 11, 22, RW, and MLS-1 through 5) located near a transect through the center of the plume (Figure 4.2). Since the wells were approximately screened across the upper three meters of the aquifer, model predictions were averaged over the top three layers for comparison to the measured data. Likewise, measured concentrations from the multilevel samplers were generally within the upper three meters of the aquifer (Table 4.2), so the measured values from the multilevel sampler ports were vertically averaged to obtain a single value for comparison. Most of the wells were sampled and analyzed for all four sampling periods (1993, 1994, 1996, and 1997), with the following exceptions. LB-EX-11 was dry in later years, so it was sampled only in 1993 and 1994. LB-EX-RW was sampled only in 1994, 1996, and 1997. Multilevel samplers 1 through 5 were sampled in 1996, and multilevel sampler 1 was sampled in 1997. Concentrations of electron acceptors and products were not measured in 1993. SEAM3D was calibrated to the 1993, 1994, and 1996 data, and the 1997 data was used to evaluate model predictions.

As described in Sections 4.3.4 and 4.3.5, only a certain few parameters were adjusted during calibration, and the magnitude of the necessary adjustments was small. To summarize the calibration process, based on the 1993 and 1994 data, the longitudinal dispersivity ($\alpha_x$) was reduced by 20%; the generation term and the retardation factor for Fe(II) were fit to observed data; the laboratory estimate for anaerobic decay rate was increased by a factor of three for the sulfate and iron reducers, and the composition of the NAPL was adjusted within ranges defined by the literature to match measured aqueous phase concentrations. Using the 1993, 1994, and 1996 data, the inhibition coefficients were adjusted to match measured $H_2S$ and $CH_4$ concentrations. All other parameters were obtained from field and laboratory measurements and literature values, and adjustment in their values was not required.

## 4.4 Results and Discussion

### *4.4.1 Concentrations along a transect through the center of the plume*

Measured and predicted concentrations were compared along a transect (see Figure 4.2) through the center of the plume. Figure 4.7 shows the predicted concentrations of the various model constituents at elapsed times of 850, 1180, 2020, 2230, 4000, and 6000 days after the estimated start of the gasoline leak. The first four times correspond to the four sampling periods, and the available measured data are also shown. In general, measured and predicted concentrations show reasonable agreement (Figure 4.7). Measured and predicted travel distances are in general agreement, which tends to verify the estimate of groundwater velocity, retardation coefficients, and the start date for the gasoline leak.

Measured values of the maximum concentrations of BTEX are highest in 1993, and decrease over time (Figure 4.7A-D), an effect which is captured by the NAPL dissolution algorithm of SEAM3D. Since BTEX and MTBE are much more soluble in water than the aliphatics, the NAPL mass fractions of BTEX and MTBE decrease over time as mass dissolves out of the NAPL phase. Thus the equilibrium concentrations of BTEX and MTBE diminish such that their maximum aqueous concentrations also decrease. This effect is most apparent with benzene (Figure 4.7A) and MTBE (Figure 4.7E), which have the highest solubilities in water. For MTBE, an unusually high concentration occurs in LB-EX-7 in 1994 and MLS-4 in 1996; however, measurements at the other locations reveal low concentrations and suggest that most of the MTBE has dissolved out of the NAPL by 1996. The aliphatics show an increase in maximum concentration (Figure 4.7K) from 2020 days to 6000 days, reflecting the increase in effective concentration of aliphatics in the NAPL during this time. This occurs because the aliphatics comprise a greater percentage of the remaining NAPL as the more soluble aromatics and MTBE dissolve into the aqueous phase. From 850 to 2020 days, the decrease in aliphatic concentration is due to the effect of excavation of the contaminated soil. Since SEAM3D uses Monod kinetics, biodegradation occurs quite slowly where the BTEX concentrations are small. Therefore, small concentrations of BTEX (Figure 4.7A-D) are transported down-gradient through the zone of oxygen depletion (Figure 4.7F) during the entire simulation. However, biodegradation does not

allow significant BTEX concentrations to occur beyond x = 150 m (less than 1.0 g $m^{-3}$ for toluene and less than 0.5 g $m^{-3}$ for the other BTEX).

The 1994 measurements showed depletion of $O_2$ (Figure 4.7F) and production of Fe(II) (Figure 4.7G), suggesting that biodegradation of BTEX was occurring at that time, with $O_2$ and Fe(III) acting as electron acceptors (EAs). Fe(II) production was observed only in locations of low concentrations of $O_2$, suggesting that $O_2$ was inhibiting Fe(III)-based biodegradation. This trend continued for 1996 and 1997, although Fe(II) adsorption caused the zone of Fe(II) depletion to lag behind the more rapidly moving $O_2$. For both the 1994 and 1996 sampling times, the predicted zone of $O_2$ depletion moved slightly ahead of the measured zone, although the measurements were sparse and the difference was not excessive (Figure 4.7F).

At the upgradient edge of the plume, measured $SO_4^{2-}$ concentrations were approximately 5 g $m^{-3}$, while the value approached 15 g $m^{-3}$ at the downgradient edge (Figure 4.7H). Measured concentrations of $H_2S$ were close to zero until 1996 (Figure 4.7I), indicating that significant $SO_4^{2-}$ reduction was not occurring in 1994. Since $O_2$ was already depleted, it is likely that the presence of Fe(III) was inhibiting $SO_4^{2-}$ reduction. Furthermore, the absence of $H_2S$ in 1994 suggests that the low $SO_4^{2-}$ concentrations (5 g $m^{-3}$) measured at the upgradient boundary were not due to biological $SO_4^{2-}$ reduction. Instead, $SO_4^{2-}$ may have reacted chemically with species such as Fe(II), which was present at that time. This process has been reported by other researchers (e.g. Bosma et al., 1996).

Measured production of methane (Figure 4.7J) follows the same trend as $H_2S$, indicating that $SO_4^{2-}$ reduction and methanogenesis are both inhibited through 1994. Measured values of methane actually decrease between 1996 and 1997, and the data do not yet indicate whether methanogenesis will be a significant process at the site. The maximum specific rates of substrate utilization ($\nu_{x,ls,le}^{max}$) for methanogenesis were based on the USGS estimates, which were sufficiently low (Table 4.7) such that predicted concentrations of methane do not rise above 3.0 g $m^{-3}$ at 6000 days (Figure 4.7J). Possible loss mechanisms for methane that are not accounted for in the model include mass transfer of methane to the vadose zone and oxidation by

methanotrophic bacteria. Additional field data will be required to define role of methanogenesis more accurately at Laurel Bay.

Measured concentrations of $H_2S$ and methane indicate a lag period of at least four years prior to initiation of $SO_4^{2-}$ reduction and methanogenesis. SEAM3D reproduces this lag period through the effect of the inhibition coefficients and the low initial biomass. Early in the simulation, significant concentrations of $O_2$ and Fe(III) inhibit $SO_4^{2-}$ reduction and methanogenesis. After $O_2$ and Fe(III) have been depleted, $SO_4^{2-}$ reduction begins to occur, but the rate is insignificant because the small biomass of $SO_4^{2-}$ reducers. Over time, the biomass increases to the point that significant $SO_4^{2-}$ based biodegradation occurs. Once the $SO_4^{2-}$ has been depleted, methanogenesis is no longer inhibited, and methane production begins. If microbial growth were not part of the SEAM3D model, inhibition alone would not cause the large lag period that was observed in the field (for details see Section 4.4.3). Other researchers have shown that lag periods for hydrocarbon degradation may vary from 10 days to 3.5 months as the EA process shifts among Fe(III) reduction, $SO_4^{2-}$ reduction, and methanogenesis (Vroblesky and Chapelle, 1994).

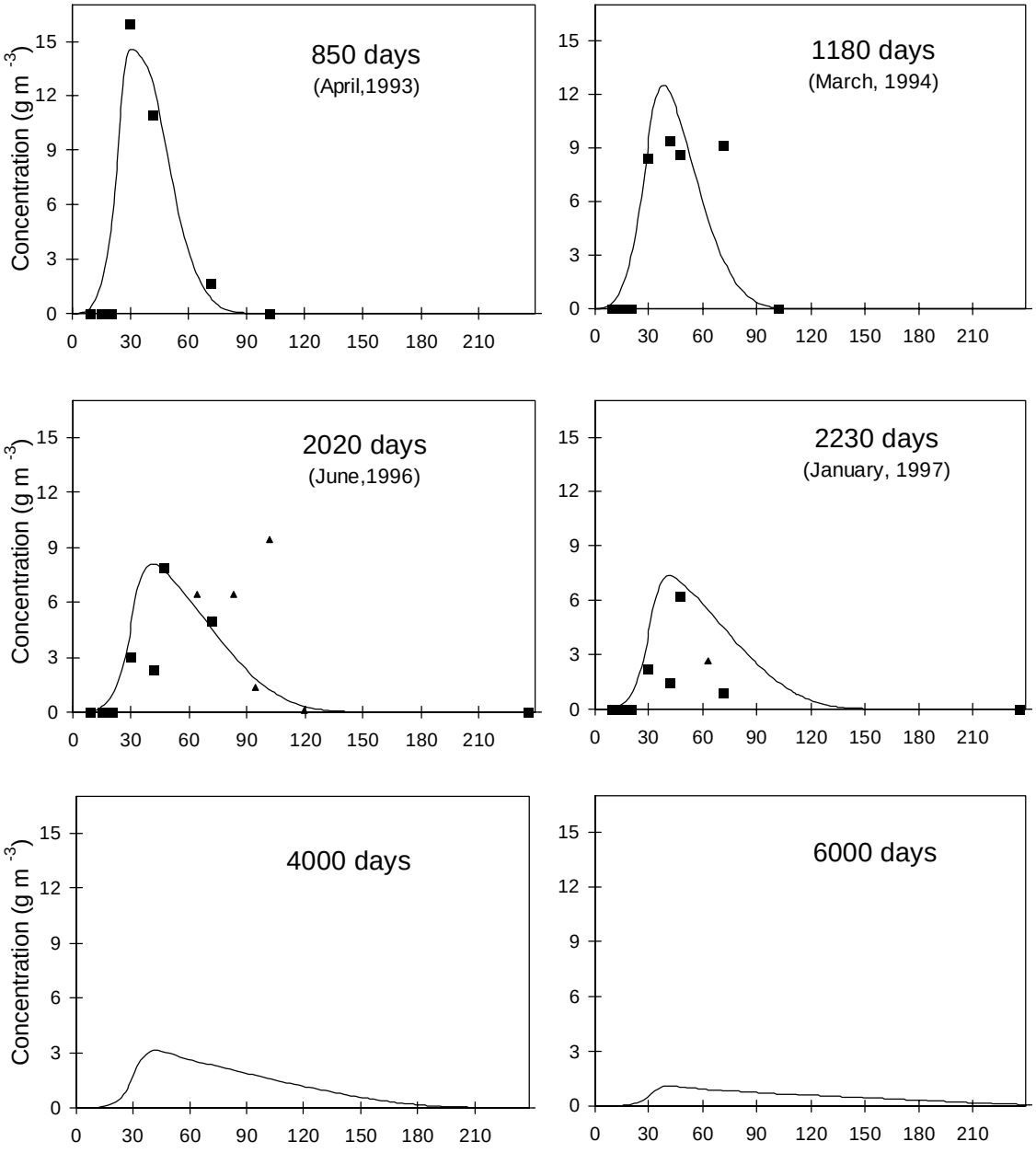


Figure 4.7 (A). Comparison of measured (symbols) and predicted (lines) concentrations along a transect through the centerline of the plume in the direction of flow for benzene. From left to right, squares correspond to monitoring wells LB-EX-5, 4, 3, 1, 7, RW, 8, and 22; while triangles correspond to multilevel samplers MLS-1, 3, 6, 4, and 5.

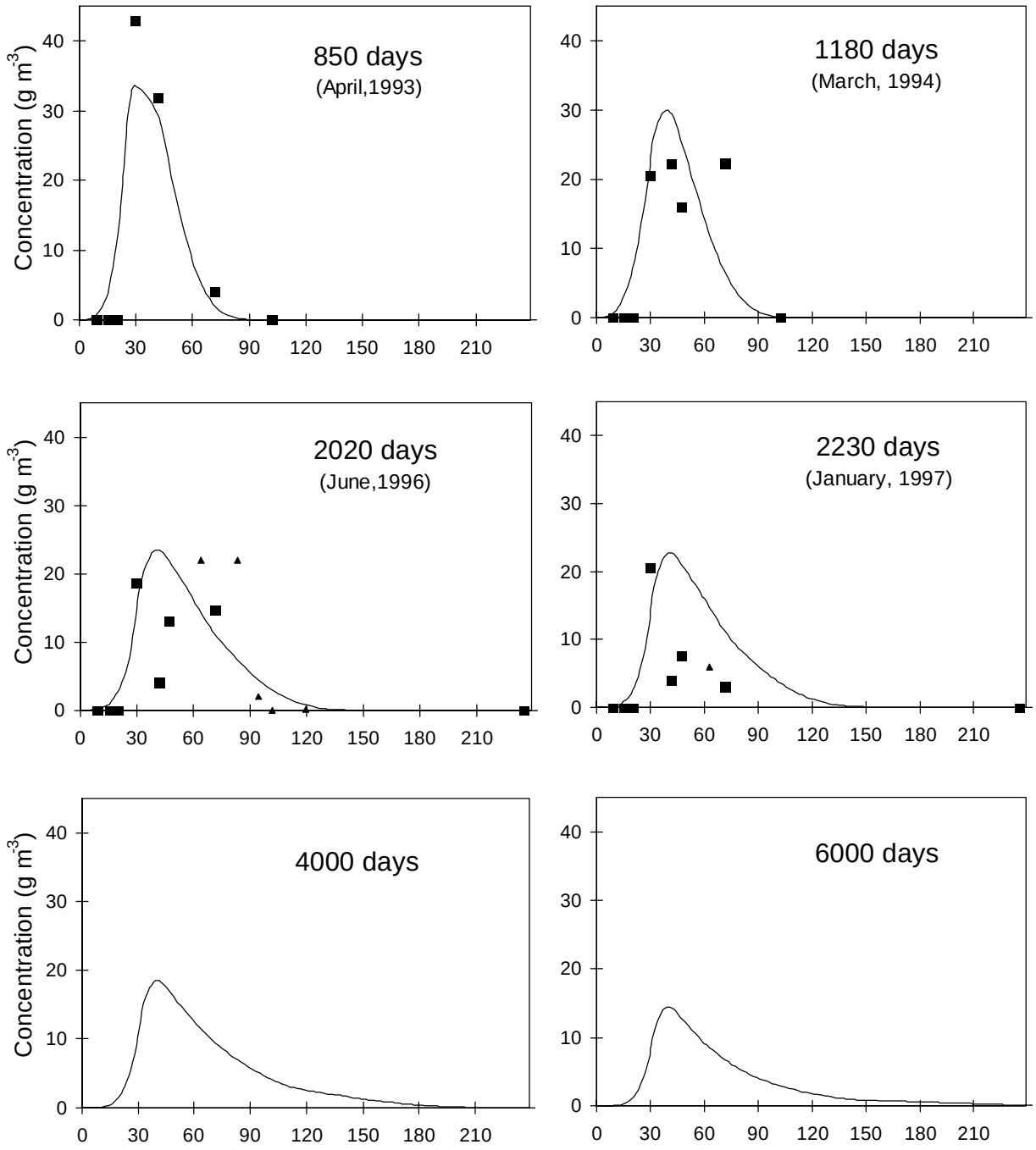


Figure 4.7 (B). Comparison of measured (symbols) and predicted (lines) concentrations along a transect through the centerline of the plume in the direction of flow for toluene. From left to right, squares correspond to monitoring wells LB-EX-5, 4, 3, 1, 7, RW, 8, and 22; while triangles correspond to multilevel samplers MLS-1, 3, 6, 4, and 5.

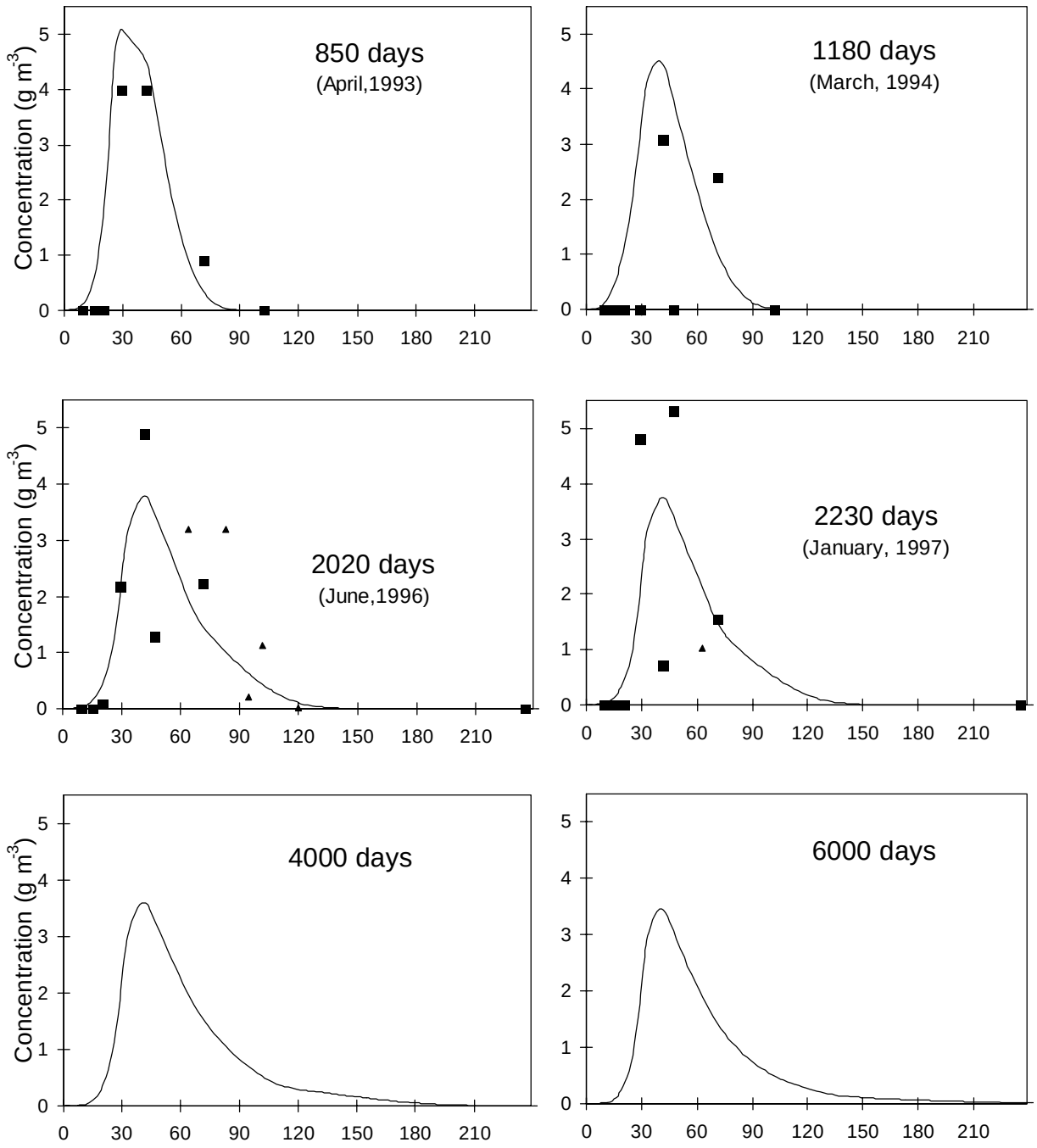


Figure 4.7 (C). Comparison of measured (symbols) and predicted (lines) concentrations along a transect through the centerline of the plume in the direction of flow for ethylbenzene. From left to right, squares correspond to monitoringwells LB-EX-5, 4, 3, 1, 7, RW, 8, and 22; while triangles correspond to multilevel samplers MLS-1, 3, 6, 4, and 5.

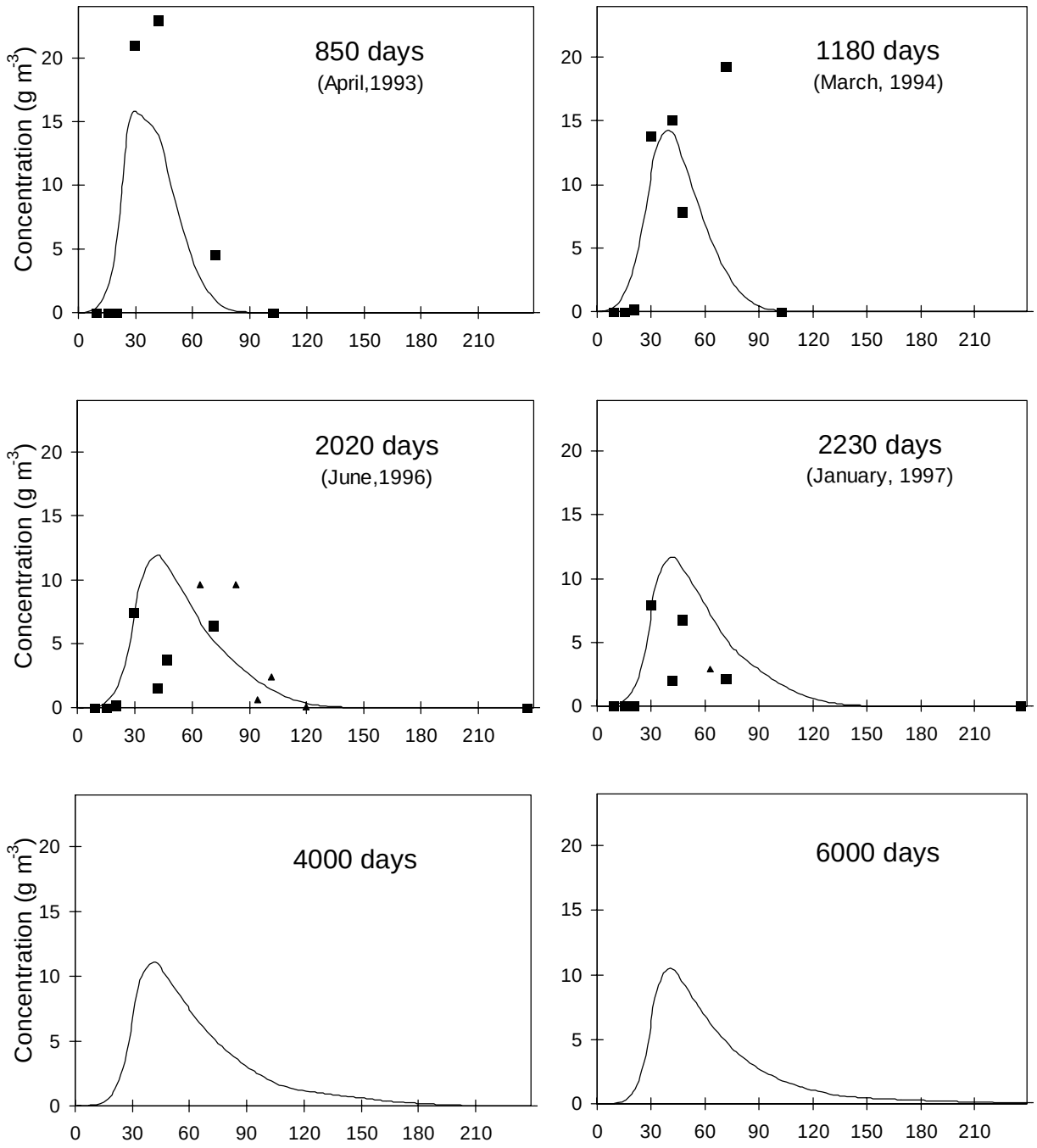


Figure 4.7 (D). Comparison of measured (symbols) and predicted (lines) concentrations along a transect through the centerline of the plume in the direction of flow for xylene. From left to right, squares correspond to monitoring wells LB-EX-5, 4, 3, 1, 7, RW, 8, and 22; while triangles correspond to multilevel samplers MLS-1, 3, 6, 4, and 5.

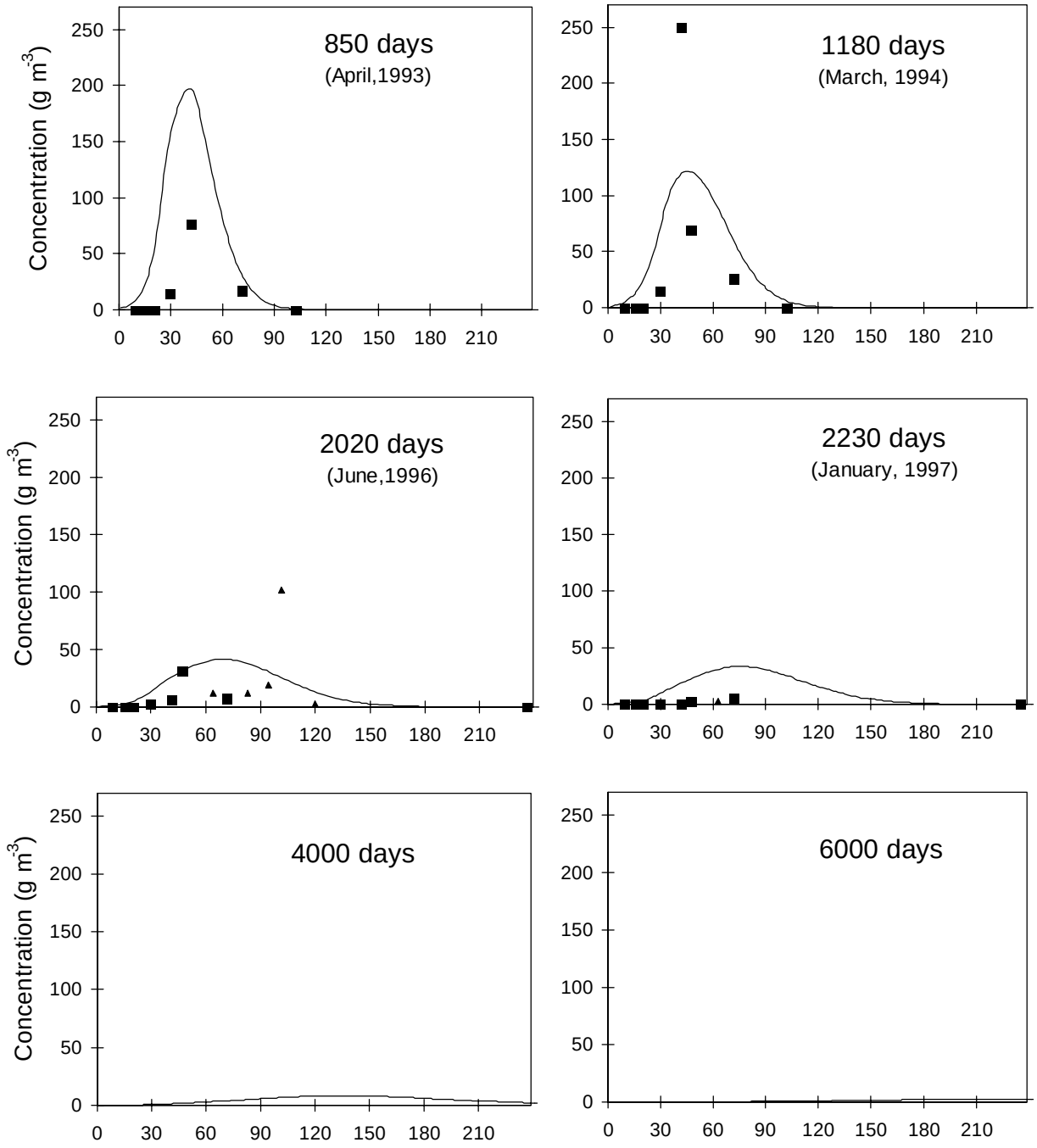


Figure 4.7 (E). Comparison of measured (symbols) and predicted (lines) concentrations along a transect through the centerline of the plume in the direction of flow for MTBE. From left to right, squares correspond to monitoring wells LB-EX-5, 4, 3, 1, 7, RW, 8, and 22; while triangles correspond to multilevel samplers MLS-1, 3, 6, 4, and 5.

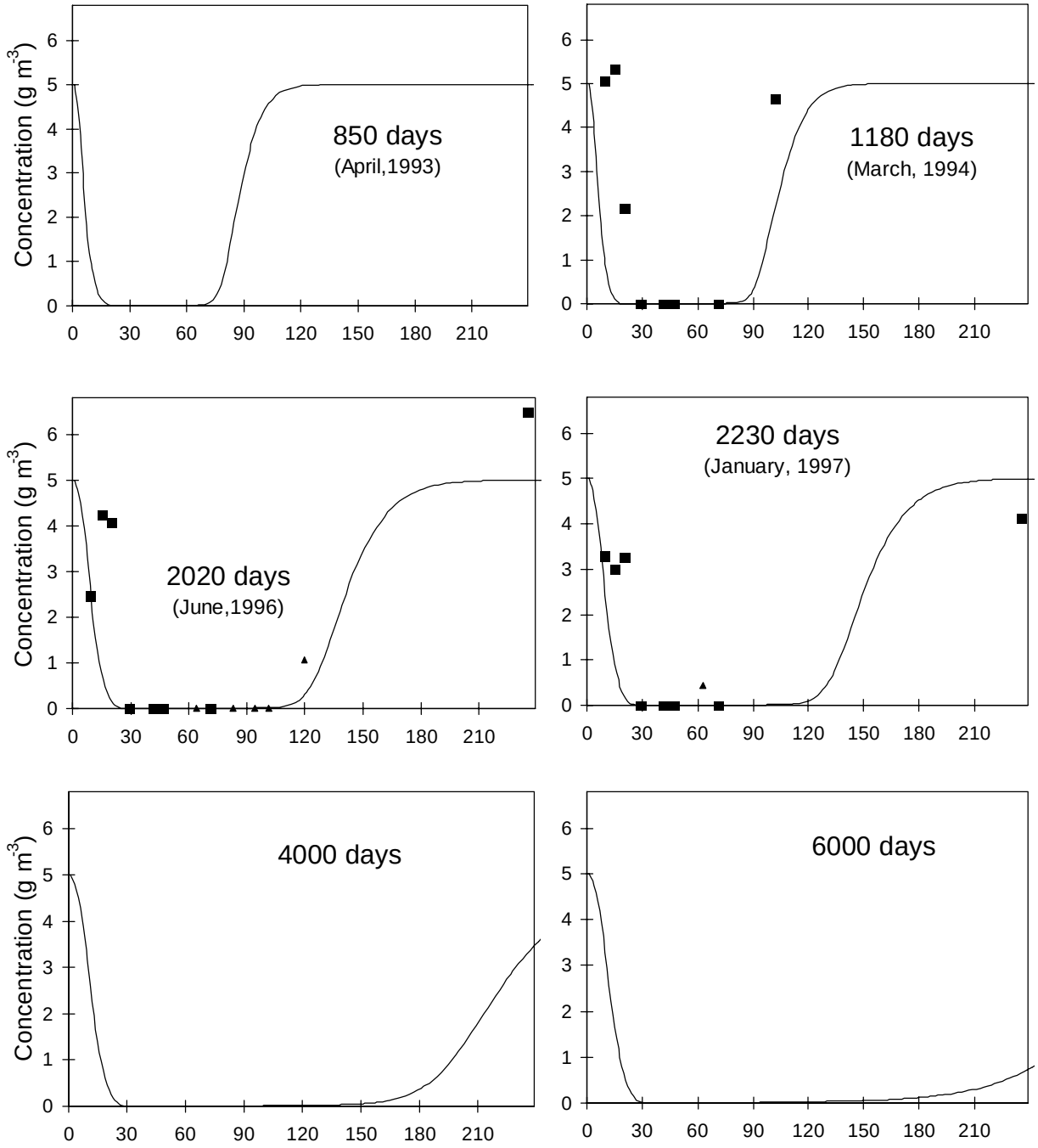


Figure 4.7 (F). Comparison of measured (symbols) and predicted (lines) concentrations along a transect through the centerline of the plume in the direction of flow for oxygen. From left to right, squares correspond to monitoring wells LB-EX-5, 4, 3, 1, 7, RW, 8, and 22; while triangles correspond to multilevel samplers MLS-1, 3, 6, 4, and 5.

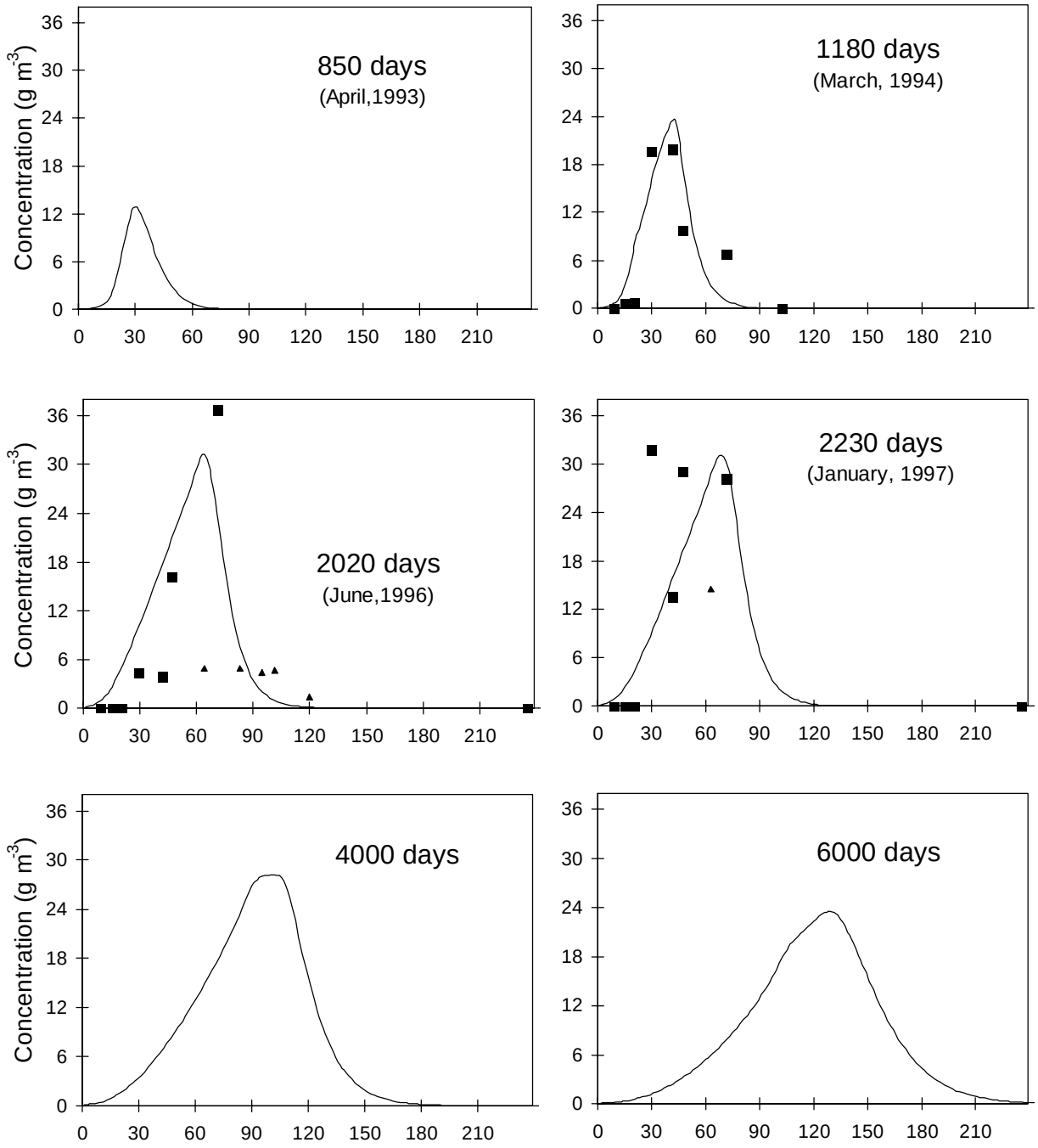


Figure 4.7 (G). Comparison of measured (symbols) and predicted (lines) concentrations along a transect through the centerline of the plume in the direction of flow for Fe(II). From left to right, squares correspond to monitoring wells LB-EX-5, 4, 3, 1, 7, RW, 8, and 22; while triangles correspond to multilevel samplers MLS-1, 3, 6, 4, and 5.

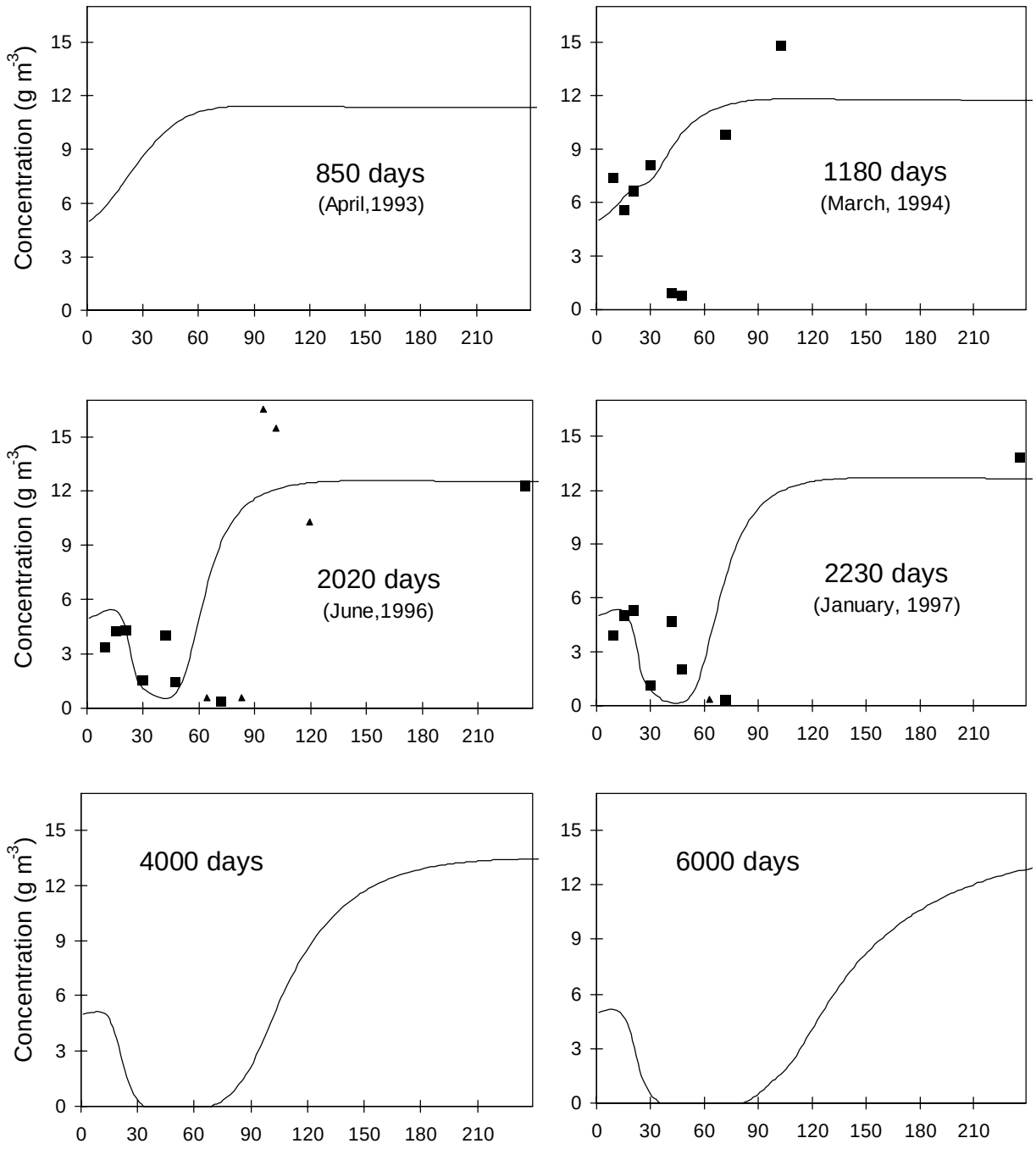


Figure 4.7 (H). Comparison of measured (symbols) and predicted (lines) concentrations along a transect through the centerline of the plume in the direction of flow for sulfate. From left to right, squares correspond to monitoring wells LB-EX-5, 4, 3, 1, 7, RW, 8, and 22; while triangles correspond to multilevel samplers MLS-1, 3, 6, 4, and 5.

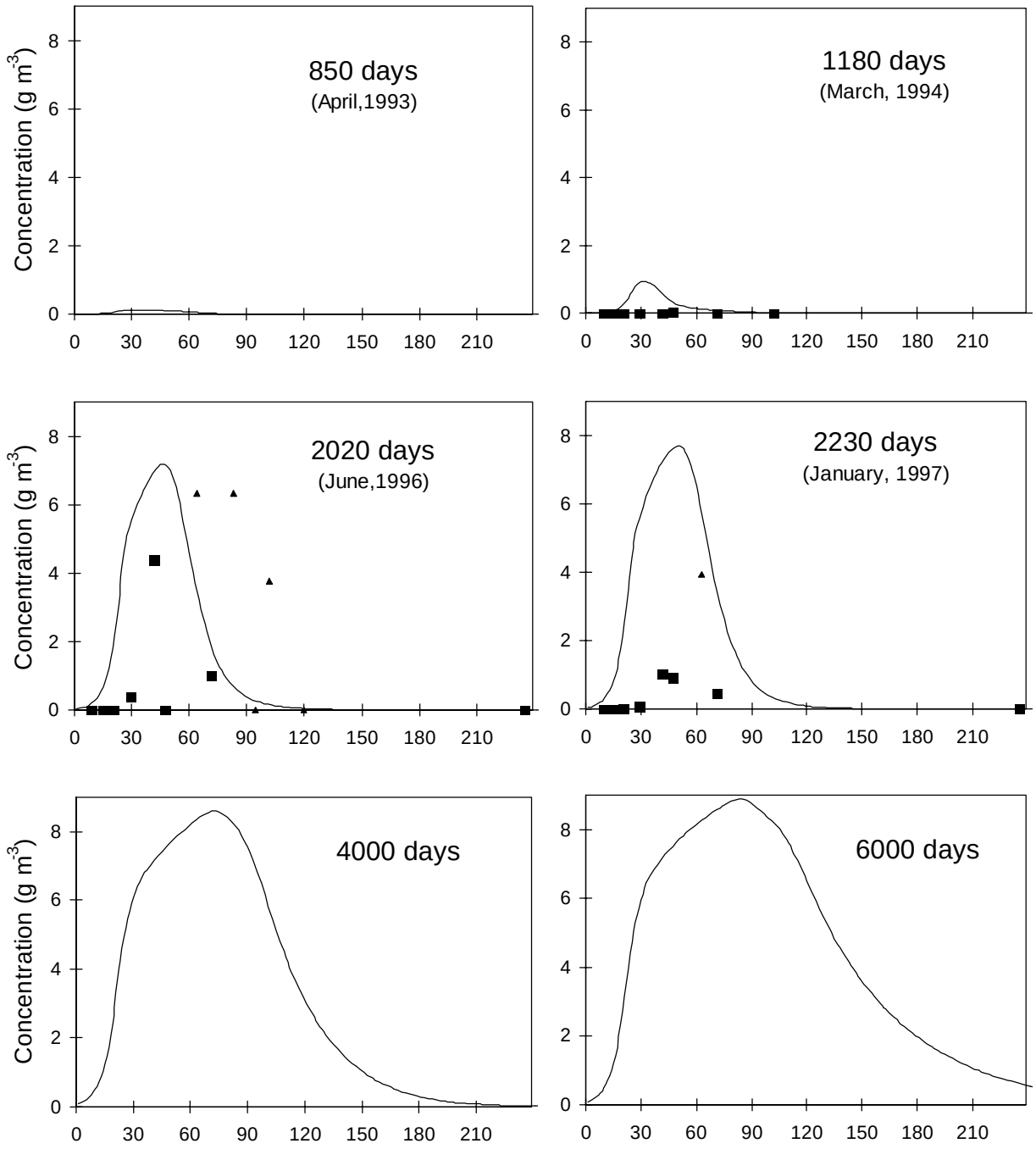


Figure 4.7 (I). Comparison of measured (symbols) and predicted (lines) concentrations along a transect through the centerline of the plume in the direction of flow for sulfide. From left to right, squares correspond to monitoring wells LB-EX-5, 4, 3, 1, 7, RW, 8, and 22; while triangles correspond to multilevel samplers MLS-1, 3, 6, 4, and 5.

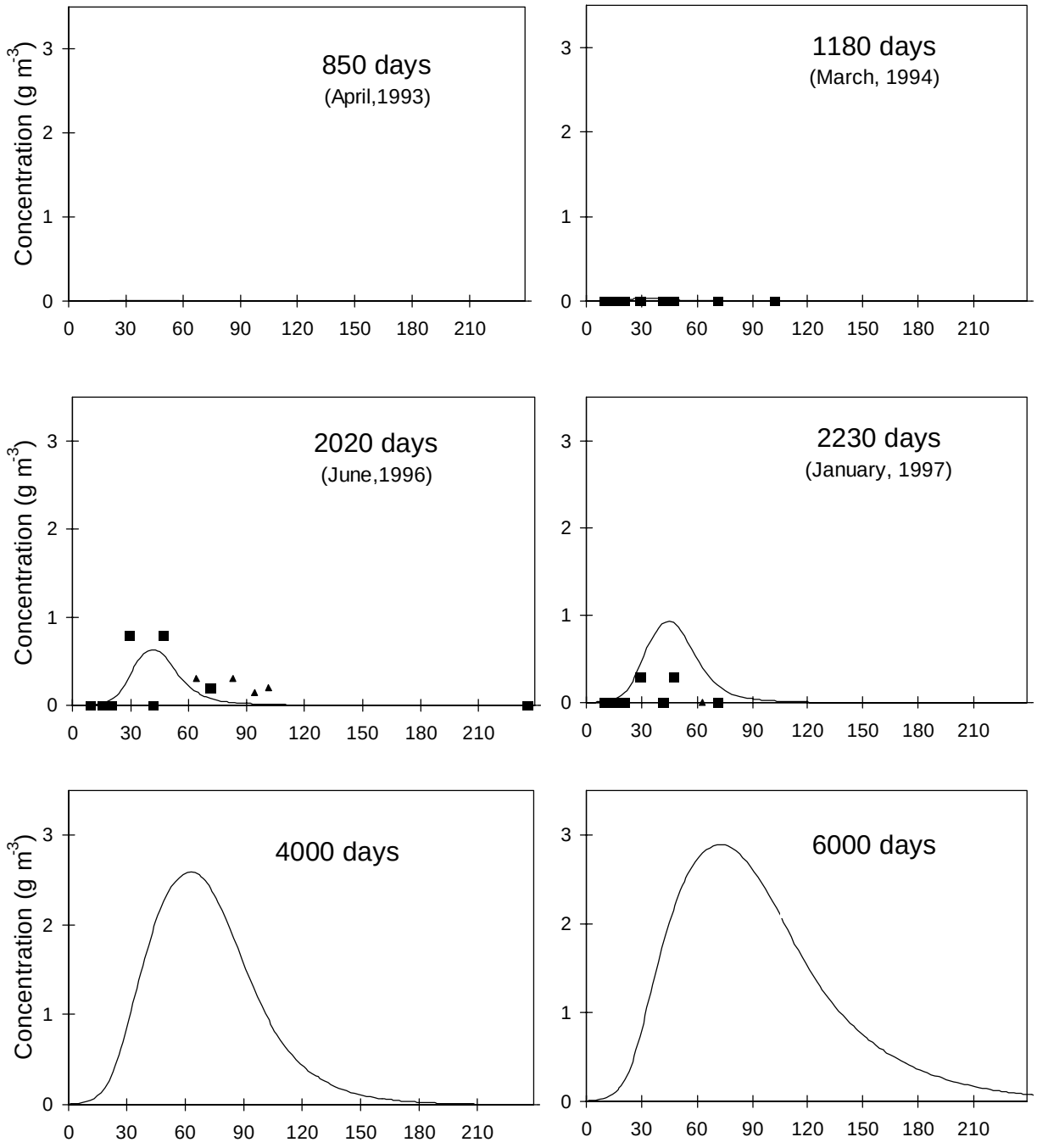


Figure 4.7 (J). Comparison of measured (symbols) and predicted (lines) concentrations along a transect through the centerline of the plume in the direction of flow for methane. From left to right, squares correspond to monitoring wells LB-EX-5, 4, 3, 1, 7, RW, 8, and 22; while triangles correspond to multilevel samplers MLS-1, 3, 6, 4, and 5.

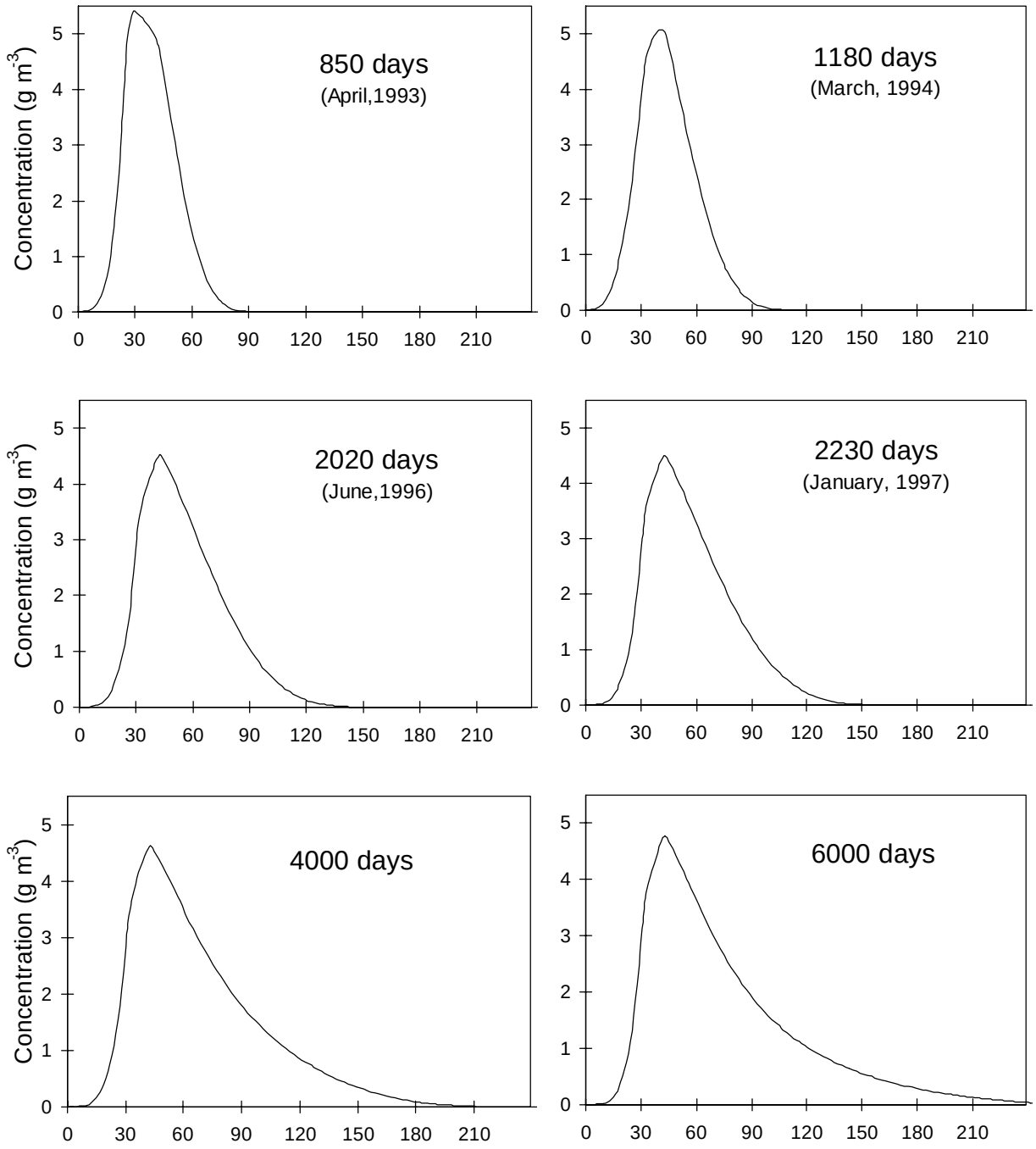


Figure 4.7 (K). Predicted concentrations along a transect through the centerline of the plume in the direction of flow for aliphatics.

### *4.4.2 Areal distributions*

The areal distributions of benzene, toluene, and MTBE at 4000 days are shown in Figure 4.8 for model layers 1, 3, 5, 7, and 9. Concentrations of benzene and toluene diminish with increasing depth, since contaminant mass must disperse from the NAPL source area to the lower layers, and significant mass remains in the NAPL. In contrast, the highest concentrations of MTBE occur in layer 5 because the majority of the MTBE has dissolved out of the NAPL phase. Thus, there is no significant source of MTBE in the upper layers, and recharge begins to dilute its concentration near the water table. BTEX spreading is limited by biodegradation and adsorption, so both hydrocarbon plumes (Figure 4.8) are narrower in the y-direction than the MTBE. In addition, the downgradient edge of the MTBE plume travels almost twice as far as the hydrocarbon plumes. Since the retardation factor for benzene and toluene is only 1.26, retardation alone does not explain the difference in travel distance, and biodegradation must contribute to the containment of the plumes.

Figure 4.9 shows the areal distributions of the electron acceptors (EAs) oxygen, solid Fe(III), and sulfate at 4000 days. As expected, EA depletion decreases with depth, reflecting the distribution of the hydrocarbons. Only small amounts of Fe(III) were utilized in the bottom layers, indicating that oxygen is inhibiting Fe(III) reduction. Since oxygen and Fe(III) inhibit sulfate use, the sulfate depletion in the bottom layer is probably caused by dispersion from the upper layers, and not by sulfate reduction in the bottom layer.

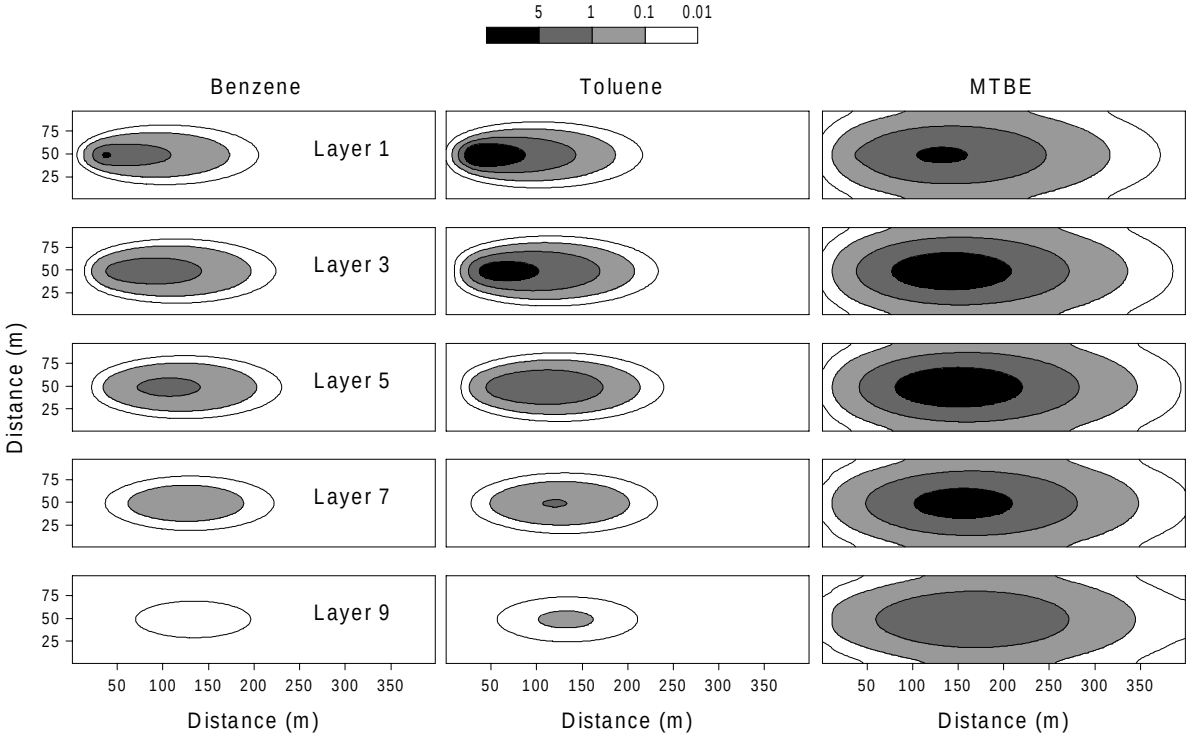


Figure 4.8. Areal contours of benzene (column 1), toluene (column 2), and MTBE (column 3) at 4000 days for model layers 1, 3, 5, 7, and 9. Units of the scale bar are g $m^{-3}$ for all three constituents.

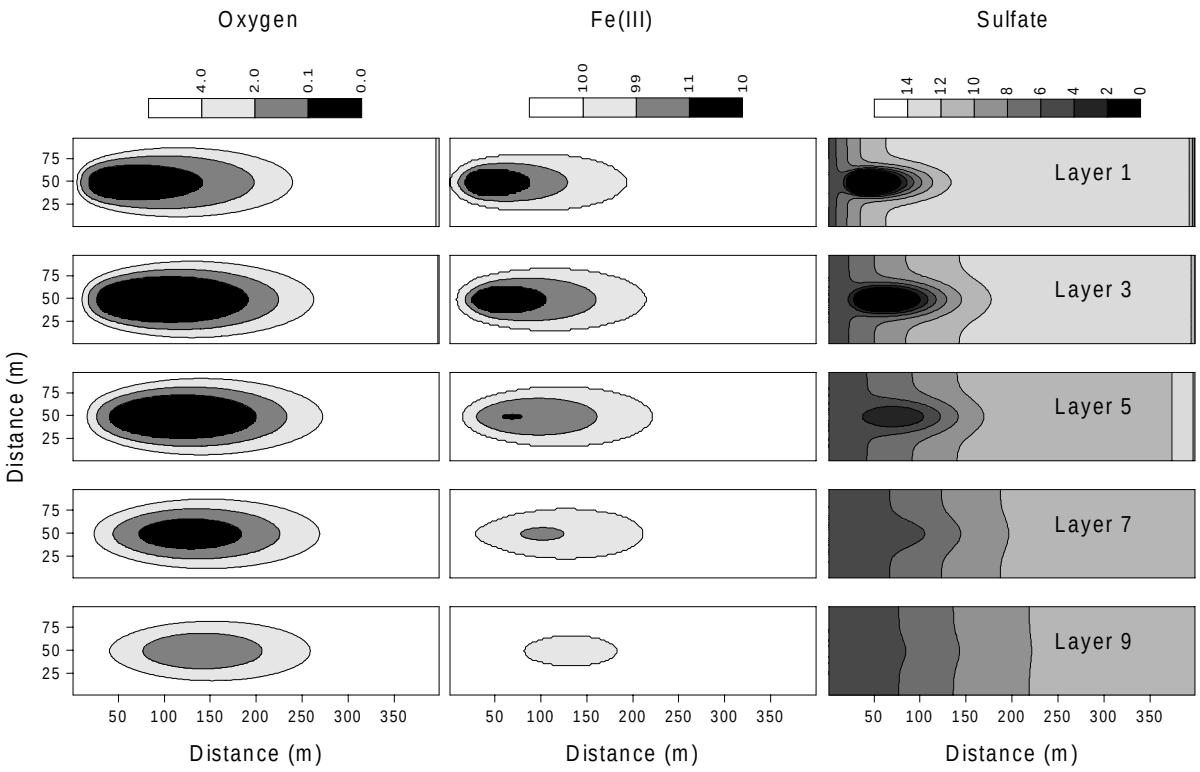


Figure 4.9. Areal contours of oxygen (column 1), Fe(III) (column 2), and sulfate (column 3) at 4000 days for model layers 1, 3, 5, 7, and 9. Units of the scale bar are g $g^{-1}$ for Fe(III) and g $m^{-3}$ for oxygen and sulfate.

### *4.4.3 Alternative model scenarios*

Since the actual NAPL concentrations in the soil were not well characterized, a theoretical worst case NAPL spill (see Section 4.3.3) was simulated to show the sensitivity of model predictions to the initial amount of gasoline in the soil. For the worst case, the initial NAPL mass per block was set twice as high as the "best estimate" case. Results of the worst case and the best estimate simulations are compared for benzene in Figure 4.10. At early times, concentrations are only slightly sensitive to the initial amount of NAPL; however, by 4000 days, the worst case spill produces concentrations that are twice as high as the best estimate spill. Thus the worst case NAPL distribution produces aqueous contamination for longer periods of time, reflecting the concept that larger NAPL spills may require longer remediation times.

As an alternative to injecting mass of NAPL over time, an equivalent mass of NAPL was injected at time zero to simulate an instantaneous spill. This simplified approach may be warranted for sudden spills, or spills in which the leak time for NAPL is much smaller than the time for aqueous phase transport and biodegradation. In this case, the instantaneous spill places NAPL approximately 20 m downgradient of the gasoline leak at initial time. Thus the overall travel distance at 850 days is overpredicted (Figure 4.10) by 20 m. However, after 2000 days, there is little difference in the instantaneous spill and the time dependent spill, as dispersion and biodegradation have greater influence on transport than advection.

For the final alternative modeling scenario, microbial growth was eliminated from the SEAM3D simulation. The initial concentrations ($M_x$) of all microbial populations were set to 0.35 g $m^{-3}$, which was equal to the value of the effective porosity ($\theta$). Thus the terms $M_x$ and $\theta$ cancel out of equations 2.5 through 2.10, such that the $R_{sink}^{bio}$ and the $R_{source}^{bio}$ terms depend only on the utilization rates ($r_x$). Without microbial growth, sulfate reducers begin to use hydrocarbon and produce significant amounts of $H_2S$ by 850 days (Figure 4.11). By 6000 days, there is little difference in the growth and no growth scenarios, as sulfate depletion limits continues production of $H_2S$. While the difference in benzene concentrations is small at 850 days (Figure4.12), the no growth scenario leads to greater biodegradation of benzene than the growth scenario at later times.

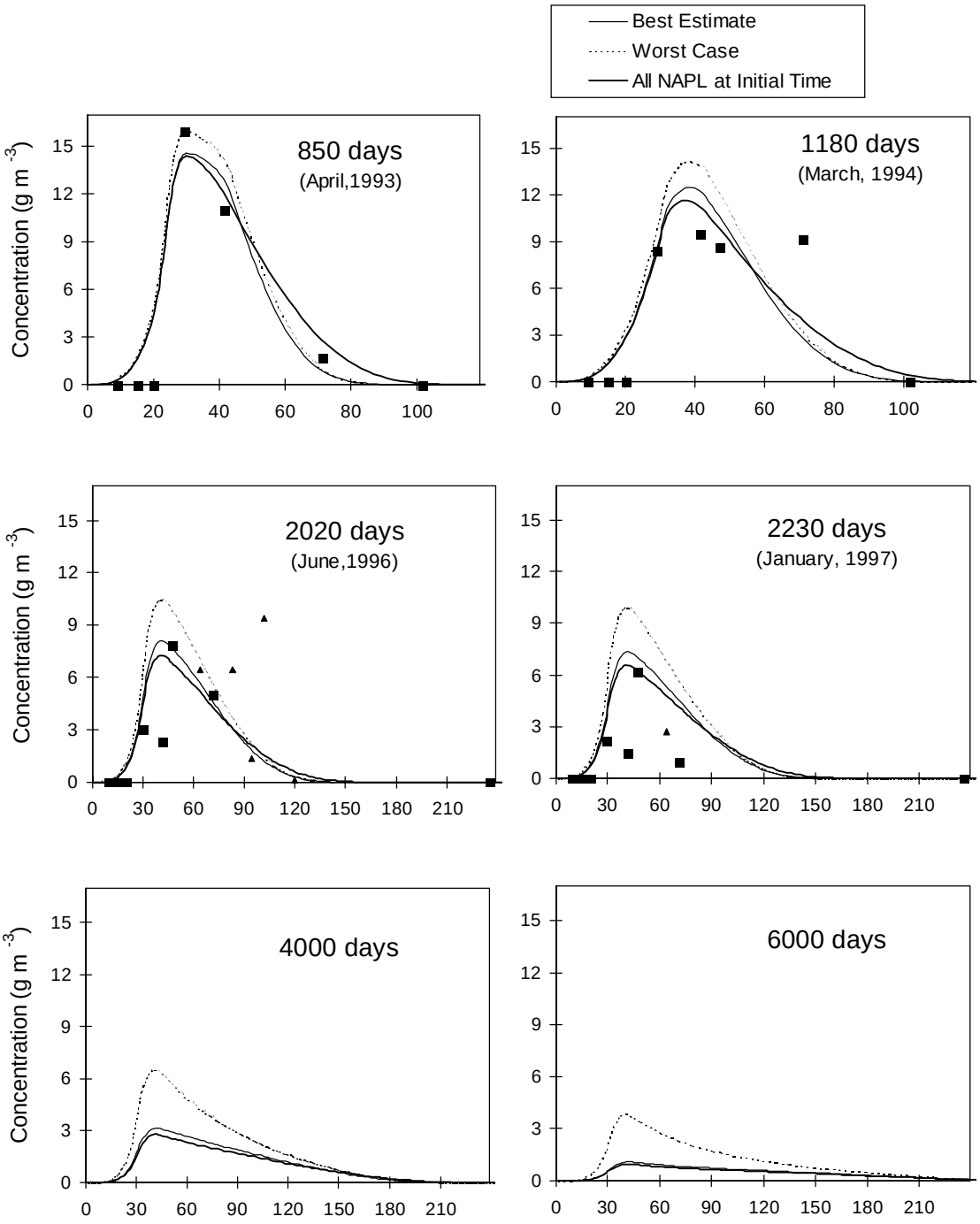


Figure 4.10. Comparison of benzene concentrations along a transect through the centerline of the plume as predicted by SEAM3D for the best estimate NAPL distribution (light solid lines), the worst case NAPL distribution (dashed lines), and entire NAPL distribution applied at initial time (heavy solid lines).

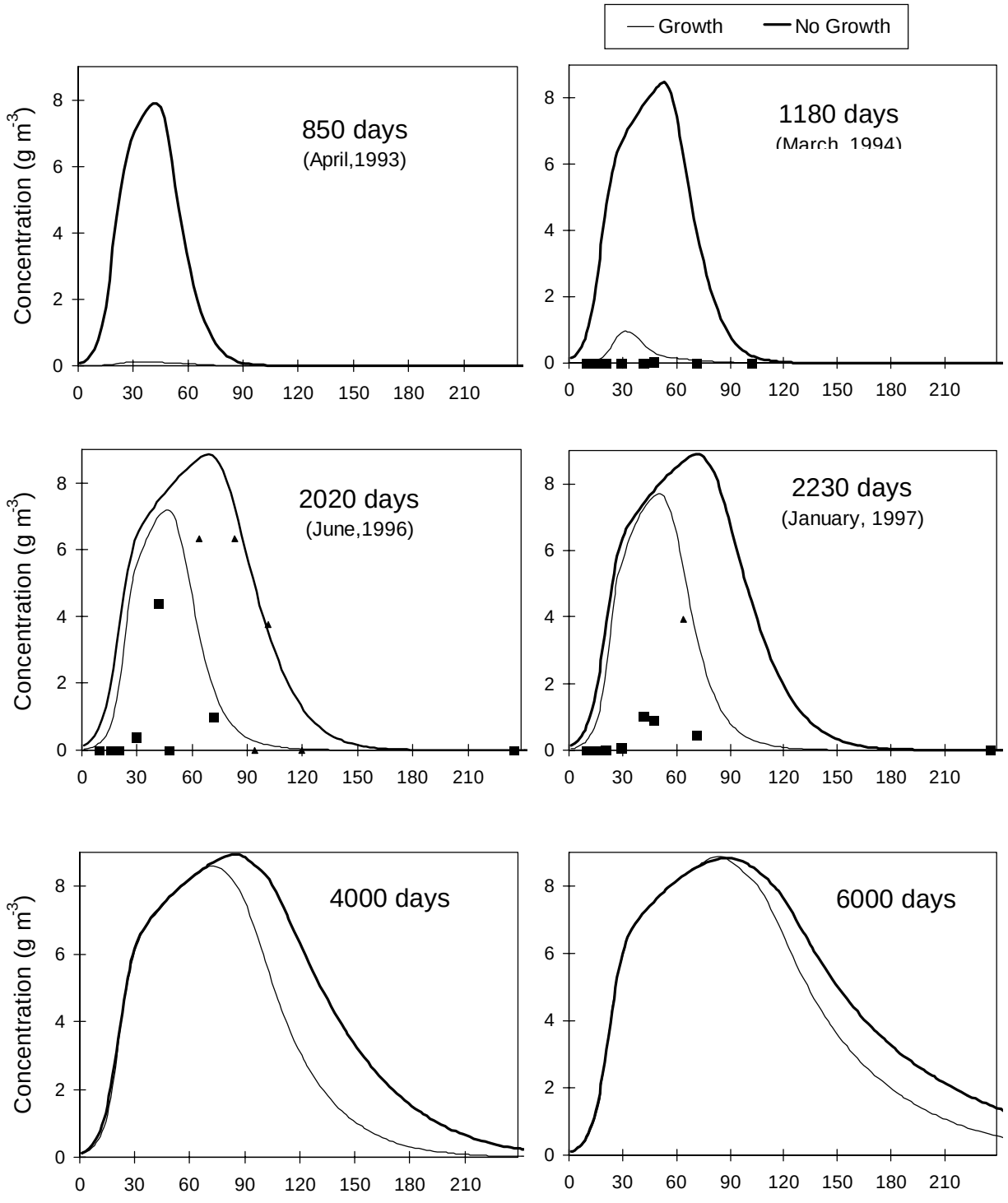


Figure 4.11. Comparison of sulfide concentrations along a transect through the centerline of the plume as predicted by SEAM3D using microbial growth (light lines) versus no microbial growth (heavy lines).

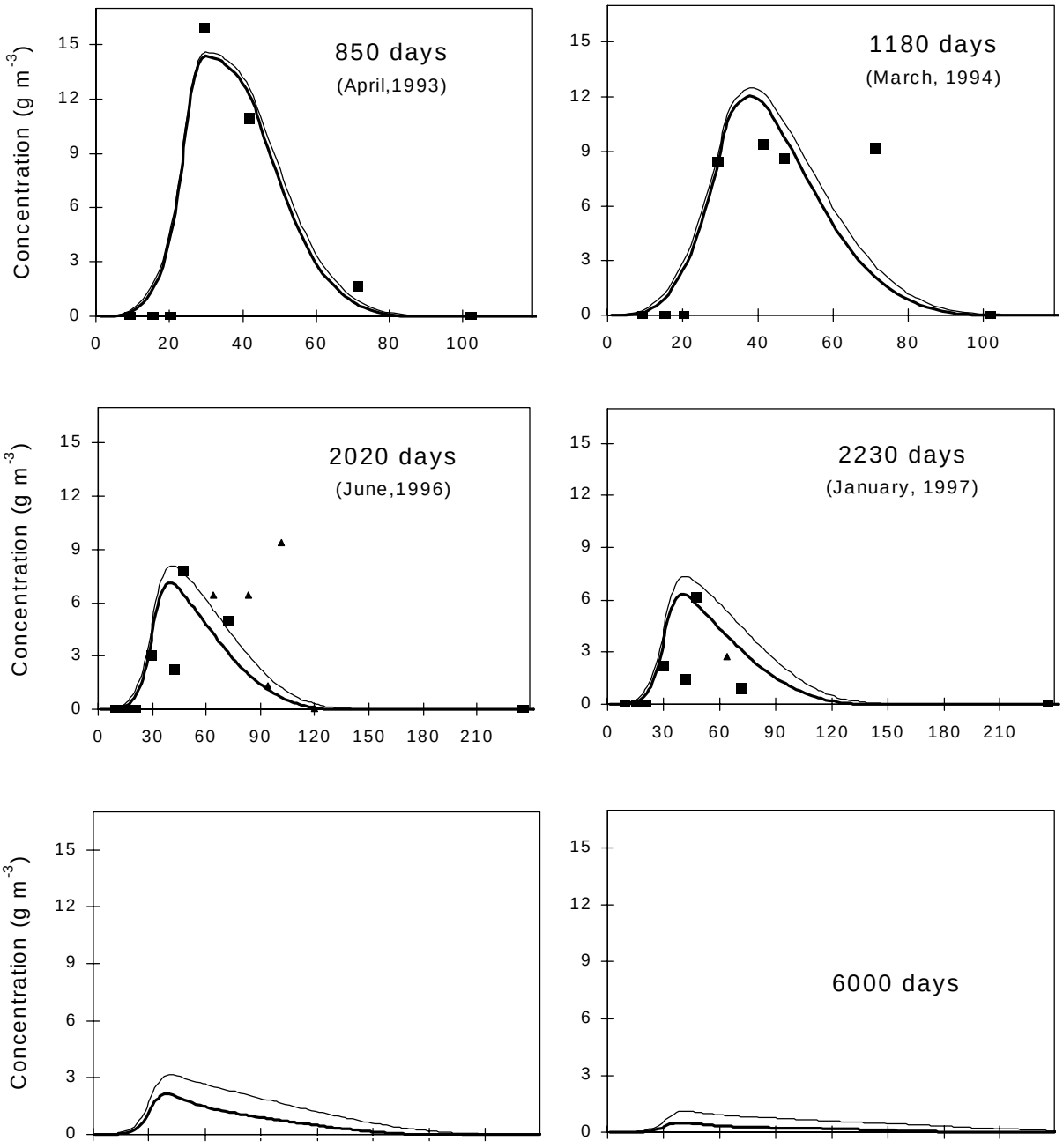


Figure 4.12. Comparison of benzene concentrations along a transect through the centerline of the plume as predicted by SEAM3D using microbial growth (light lines) versus no microbial growth (heavy lines).

## 4.5 Conclusions

In modeling contaminant transport following a gasoline spill, SEAM3D captured the trends of BTEX biodegradation without requiring significant adjustment of parameters during calibration. Biodegradation based on multiple electron acceptors was shown to limit BTEX concentrations and travel distance in directions transverse to average flow as well as in the flow direction. At early times, maximum concentrations of contaminant were not sensitive to the mass of NAPL spilled. However, at later times, the larger initial NAPL mass distribution produced higher contaminant concentrations. The microbial growth process allowed SEAM3D to capture the effect of time lags in biodegradation due to shifting electron acceptor processes. As the overall simulation time became much greater than the lag times, the effect of the lag became insignificant. A similar effect occurred in simulating the actual leak of NAPL into the subsurface. The timing of the NAPL leak was important early in the simulation, but the significance of the timing of the leak diminished as the simulation time became much greater than the leak duration. The results suggest that the most complex modeling approach is justified when the goal is to simulate biodegradation in close proximity to a NAPL spill or soon after a spill has occurred.